Signatures of Lifshitz transition in the optical conductivity of two-dimensional tilted Dirac materials

Chao-Yang Tan,[1,2,*] Jian-Tong Hou,[3,1,*] Chang-Xu Yan,[1] Hong Guo,[4,1] and Hao-Ran Chang (张浩然)[1,3,4,†]

[1]*Department of Physics, Institute of Solid State Physics and Center for Computational Sciences, Sichuan Normal University, Chengdu, Sichuan 610066, China*

[2]*Department of Physics and Beijing Key Laboratory of Opto-electronic Functional Materials and Micro-nano Devices, Renmin University of China, Beijing 100872, China*

[3]*College of Physical Science and Technology, Sichuan University, Chengdu, Sichuan 610064, China*

[4]*Department of Physics, McGill University, Montreal, Quebec, Canada H3A 2T8*

(Received 17 December 2021; revised 31 July 2022; accepted 26 September 2022; published 4 October 2022)

Lifshitz transition is a kind of topological phase transition in which the Fermi surface is reconstructed. It can occur in the two-dimensional (2D) tilted Dirac materials when the energy bands change between the type-I phase ($0 < t < 1$) and the type-II phase ($t > 1$) through the type-III phase ($t = 1$), where different tilts are parametrized by the values of t. In order to characterize the Lifshitz transition therein, we theoretically investigate the longitudinal optical conductivities (LOCs) in type-I, type-II, and type-III Dirac materials within linear response theory. In the undoped case, the LOCs are constants either independent of the tilt parameter in both type-I and type-III phases or determined by the tilt parameter in the type-II phase. In the doped case, the LOCs are anisotropic and possess two critical frequencies determined by $\omega = \omega_1(t)$ and $\omega = \omega_2(t)$, which are also confirmed by the joint density of state. The tilt parameter and chemical potential can be extracted from optical experiments by measuring the positions of these two critical boundaries and their separation $\Delta\omega(t) = \omega_2(t) - \omega_1(t)$. With increasing the tilting, the separation becomes larger in the type-I phase whereas smaller in the type-II phase. The LOCs in the regime of large photon energy are exactly the same as that in the undoped case. The type of 2D tilted Dirac bands can be determined by the asymptotic background values, critical boundaries, and their separation in the LOCs. These can therefore be taken as signatures of Lifshitz transition therein. The results of this work are expected to be qualitatively valid for a large number of 2D tilted Dirac materials, such as 8-*Pmmn* borophene monolayer, α-SnS_2, $TaCoTe_2$, $TaIrTe_4$, and $1T'$ transition metal dichalcogenides, due to the underlying intrinsic similarities of 2D tilted Dirac bands.

DOI: 10.1103/PhysRevB.106.165404

I. INTRODUCTION

Graphene has triggered extremely active research in two-dimensional (2D) Dirac materials characterized by linear and/or hyperbolic energy dispersions around Dirac points in momentum space [1,2], such as α-$(BEDT\text{-}TTF)_2I_3$ [3], silicene [4–8], graphene under uniaxial strain [9], 8-*Pmmn* borophene [10–13], transition metal dichalcogenides [14–16], partially hydrogenated graphene [17], α-SnS_2 [18], $TaCoTe_2$ [19], and $TaIrTe_4$ [20]. Among them, 2D tilted Dirac materials host tilted dispersions along a certain direction of wave vector and have been attracting increasing interests theoretically and experimentally [3,9–13,16–20]. They exhibit many significant qualitative differences in physical behaviors compared to their untilted counterparts, including plasmons [21–26], optical conductivities [22,26–34], Weiss oscillation [35], spectrum of superconducting excitations [36], Klein tunneling [37–39], Kondo effects [40], Ruderman-Kittel-Kasuya-Yosida (RKKY) interactions [41,42], Hall effects [43,44], thermoelectric effects [45], thermal currents [46], valley filtering [47], gravitomagnetic effects [48], Andreev reflection [49], Coulomb bound states [50], guided modes [51], and valley-dependent time evolution of coherent electron states [52].

Lifshitz transition is a kind of topological phase transition in which the Fermi surface is reconstructed [53], which is crucial for understanding the novel states of matter and physical properties around the transition. It accounts for the huge magnetoresistance in black phosphorus [54], superconductivity in iron-based superconductors [55–59], and abnormal transport behavior in heavy fermion materials and topological quantum materials [60–63]. The Lifshitz transition occurs in tilted Dirac materials when the energy bands change between the type-I phase (undertilted, $0 < t < 1$) and the type-II phase (overtilted, $t > 1$) through the type-III phase (critical tilted, $t = 1$) where t is the tilt parameter [64,65]. In three-dimensional (3D) tilted Dirac bands, many physical properties can characterize the Lifshitz transition, such as spin susceptibilities [66], magnetic response [67,68], Hall conductivity [69], anomalous Nernst effect [70,71], magnetoresponse [72], Andreev reflection [73], Klein tunneling [74], Kerr rotation [75], magnetothermal transport [76], plasmon [77], RKKY interaction [78], and optical response [79–81].

Similarly, the Lifshitz transition can be realized in 2D tilted Dirac materials. For example, 8-*Pmmn* borophene undergoes

*These authors contributed equally to this work.
†Corresponding author: hrchang@mail.ustc.edu.cn

the Lifshitz transition under the control of tunable vertical electrostatic field [82]; the different compounds in $1T'$ transition metal dichalcogenides correspond to different phases of the Lifshitz transition [16]: type-I phase ($1T'$-MoS_2 and $1T'$-$MoSe_2$), type-III phase ($1T'$-WSe_2), and type-II phase ($1T'$-$MoTe_2$ and $1T'$-WTe_2). Consequently, a very important issue is how to most effectively characterize the Lifshitz transition in 2D tilted Dirac materials. In 2D tilted Dirac bands, some indicators were already proposed to characterize the Lifshitz transition, including the spectrum of superconducting excitations [36], Coulomb bound states [50], and nonlinear optical response [81].

The optical conductivity provides a powerful method for extracting the information of energy band structure, and has been extensively investigated theoretically and experimentally in the 2D *untilted* Dirac bands [83–96] and undertilted Dirac bands [22,26–31]. Specifically, the exotic behaviors of longitudinal optical conductivity (LOC) can be used to characterize the topological phase transitions in both silicene [90] and $1T'$-MoS_2 [30]. However, the energy bands of the above-mentioned 2D Dirac materials are restricted to either the untilted or the undertilted (type-I phase), leaving the impact of type-II and type-III energy bands on the LOCs unexplored. To characterize the Lifshitz transition of tilted Dirac materials, we perform a comprehensive study of the LOCs in the type-I, type-II, and type-III phases. In particular, we focus our theoretical study of LOCs on both the undoped and doped situations.

The rest of the paper is organized as follows. In Sec.II, we briefly describe the model Hamiltonian and theoretical formalism to calculate the LOC. The analytical expressions for the interband conductivity, joint density of states (JDOS), and the results for interband conductivity are presented in Sec. III and Sec. IV, respectively. In addition, the intraband conductivities are analytically calculated in Sec. V. The summary and conclusions are given in Sec. VI. Finally, we present four appendices to show detailed calculations.

II. THEORETICAL FORMALISM

We begin with the Hamiltonian in the vicinity of one of two valleys for 2D tilted Dirac materials [3,9–13,22]

$$\mathcal{H}_\kappa(k_x, k_y) = \kappa\hbar v_t k_y \tau_0 + \hbar(v_x k_x \tau_1 + v_y k_y \tau_2), \tag{1}$$

where $\kappa = \pm$ labels two valleys, $k = (k_x, k_y)$ stands for the wave vector, and τ_0 and τ_i denote the 2×2 unit matrix and Pauli matrices, respectively. For simplicity, we hereafter set $\hbar = 1$ and introduce the tilt parameter t by defining

$$t = \frac{v_t}{v_y}. \tag{2}$$

It is noted that this system remains invariant under the valley transformation $(\kappa, k_y) \leftrightarrow (-\kappa, -k_y)$, indicating $\mathcal{H}_{-\kappa}(k_x, -k_y) = \mathcal{H}_\kappa(k_x, k_y)$. The eigenvalue evaluated from the Hamiltonian reads

$$\varepsilon_\kappa^\lambda(k_x, k_y) = \kappa t v_y k_y + \lambda \mathcal{Z}(k_x, k_y), \tag{3}$$

where $\mathcal{Z}(k_x, k_y) = \sqrt{v_x^2 k_x^2 + v_y^2 k_y^2}$, and $\lambda = \pm 1$ denotes the conduction band ($\lambda = +1$) and valence band ($\lambda = -1$), respectively. The energy bands and the Fermi surfaces for the n-doped case at the $\kappa = +$ valley, are schematically shown in Fig. 1.

For the untilted case ($t = 0$), the only Fermi surface, contributed completely by the electron pocket with a closed area [see Figs. 1(a) and 1(e)], is an ellipse obeying the equation

$$\frac{k_x^2}{\frac{\mu^2}{v_x^2}} + \frac{k_y^2}{\frac{\mu^2}{v_y^2}} = 1, \tag{4}$$

which reduces to a circle when $v_x = v_y$. For the type-I phase ($0 < t < 1$), the only Fermi surface, also contributed completely by the closed electron pocket [see Figs. 1(b) and 1(f)], is an ellipse obeying the equation

$$\frac{k_x^2}{\frac{\mu^2}{v_x^2(1-t^2)}} + \frac{\left(k_y + \frac{\kappa t\mu}{v_y(1-t^2)}\right)^2}{\frac{\mu^2}{v_y^2(1-t^2)^2}} = 1, \tag{5}$$

which remains an ellipse even when $v_x = v_y$. The tilt parameter t moves the center of the ellipse along the k_y axis and changes the major axis and minor axis of the ellipse. For the type-III phase ($t = 1$), the only Fermi surface, contributed entirely by the electron pocket with an open border [see Figs. 1(c) and 1(g)], is a parabola satisfying

$$k_y = \frac{\mu}{2\kappa v_y} - \frac{v_x^2 k_x^2}{2\kappa\mu v_y}. \tag{6}$$

Interestingly, for the type-II phase ($t > 1$), the Fermi surface is a couple of hyperbola [see Figs. 1(d) and 1(h)] whose equation reads

$$\frac{\left(k_y - \frac{\kappa t\mu}{v_y(t^2-1)}\right)^2}{\frac{\mu^2}{v_y^2(t^2-1)^2}} - \frac{k_x^2}{\frac{\mu^2}{v_x^2(t^2-1)}} = 1, \tag{7}$$

which is contributed not only by the electron pocket but also by the hole pocket.

These indicate that the Fermi surface is reconstructed when the energy band changes between the type-I phase and the type-II phase, corresponding to a Lifshitz transition [see Figs. 1(e)–1(h)]. On the other hand, the edges of the electron pocket and the hole pocket determine the boundaries of the interband transition of the LOCs. As a consequence, the Lifshitz transition can be characterized by the critical boundaries of interband conductivity. It is the purpose of this work to characterize such Lifshitz transition in the 2D tilted Dirac materials via the LOC.

Within linear response theory, the LOC $\sigma_{jj}(\omega)$ at finite photon frequency ω is given by

$$\sigma_{jj}(\omega) = g_s \sum_{\kappa=\pm1} \sigma_{jj}^\kappa(\omega), \tag{8}$$

where $j = x, y$ stands for the spatial component, $g_s = 2$ represents the spin degeneracy, and $\sigma_{jj}^\kappa(\omega)$ denotes the LOC at given valley κ, whose explicit expression is provided in Appendix A. Interestingly, $\sigma_{jj}(\omega)$ possesses the particle-hole symmetry (see Appendix A for details) such that we can safely replace μ by $|\mu|$ in all of $\sigma_{jj}(\omega)$, $\sigma_{jj}^\kappa(\omega)$, and $f(x)$ because we only concern the final result of $\sigma_{jj}(\omega)$. It can be proven that $\sigma_{jj}^\kappa(\omega) = \sigma_{jj}^{-\kappa}(\omega)$ by considering $\mathcal{H}_{-\kappa}(k_x, -k_y) =$

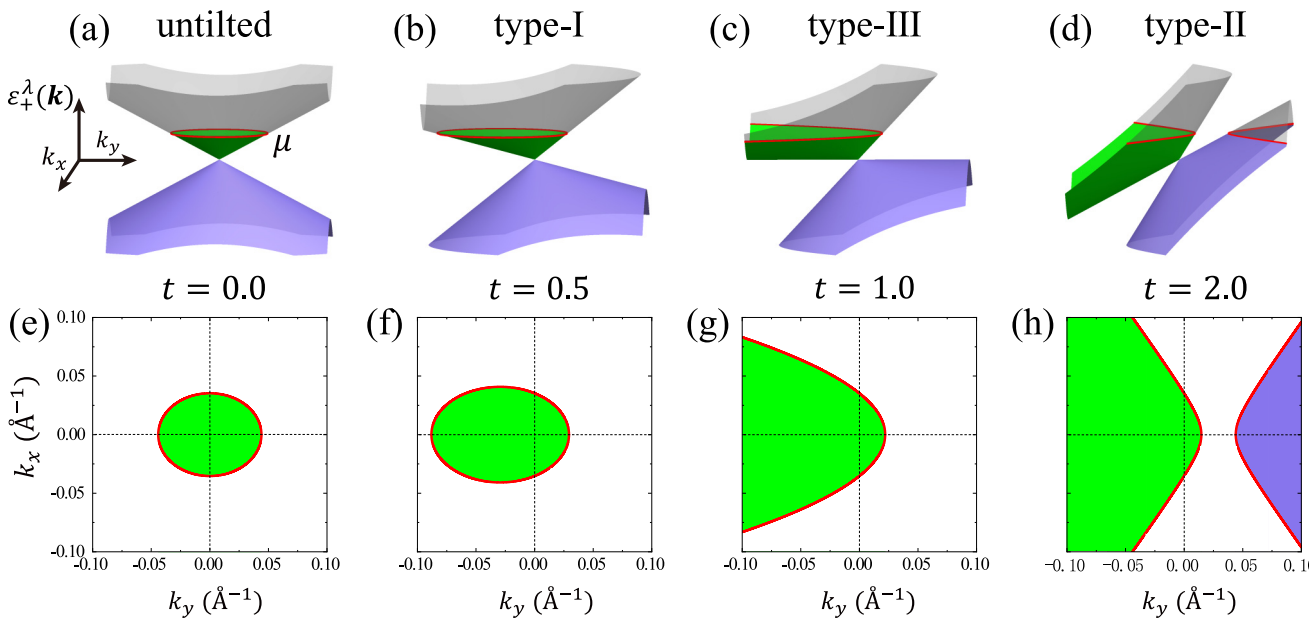

FIG. 1. Schematic diagrams for tilted Dirac bands (top panels) and the corresponding Fermi surfaces (bottom panels) of different typical tilt parameters t at the $\kappa = +$ valley. The green and purple shaded regions represent electron and hole pockets, respectively. The Fermi contour represented by the red line, is an ellipse for $t = 0$ and $t = 0.5$, a parabola for $t = 1$, and a couple of hyperbola for $t = 2$. We hereafter set the chemical potential $\mu = 0.2$ eV and the Fermi velocities $v_x = 0.86v_F$, $v_y = 0.69v_F$ with $v_F = 10^6$ m/s, the same as that given in Ref. [27].

$\mathcal{H}_\kappa(k_x, k_y)$, such that we are allowed to focus on the $\kappa = +$ or the $\kappa = -$ valley. Hereafter, we restrict our analysis to the n-doped case ($\mu > 0$) and the $\kappa = +$ valley for convenience.

After some standard algebra, the real part of the LOCs can be divided into an interband part and an intraband part as

$$\mathrm{Re}\sigma_{jj}^{\kappa}(\omega) = \begin{cases} \mathrm{Re}\sigma_{jj(\mathrm{IB})}^{\kappa}(\omega) + \Theta[\mu]\mathrm{Re}\sigma_{jj(\mathrm{D})}^{\kappa,+}(\omega) + \Theta[-\mu]\mathrm{Re}\sigma_{jj(\mathrm{D})}^{\kappa,-}(\omega), & 0 \leqslant t \leqslant 1 \\ \mathrm{Re}\sigma_{jj(\mathrm{IB})}^{\kappa}(\omega) + \mathrm{Re}\sigma_{jj(\mathrm{D})}^{\kappa,+}(\omega) + \mathrm{Re}\sigma_{jj(\mathrm{D})}^{\kappa,-}(\omega), & t > 1, \end{cases} \tag{9}$$

where $\Theta(x)$ is the Heaviside step function satisfying $\Theta(x) = 0$ for $x \leqslant 0$ and $\Theta(x) = 1$ for $x > 0$, and μ denotes the chemical potential measured with respect to the Dirac point. In addition, the interband and intraband conductivities are given, respectively, as

$$\mathrm{Re}\sigma_{jj(\mathrm{IB})}^{\kappa}(\omega) = \pi \int_{-\infty}^{+\infty} \frac{dk_x}{2\pi} \int_{-\infty}^{+\infty} \frac{dk_y}{2\pi} \mathcal{F}_{-,+}^{\kappa;jj}(k_x, k_y) \frac{f[\varepsilon_\kappa^-(k_x, k_y)] - f[\varepsilon_\kappa^+(k_x, k_y)]}{\omega} \delta[\omega - 2\mathcal{Z}(k_x, k_y)], \tag{10}$$

$$\mathrm{Re}\sigma_{jj(\mathrm{D})}^{\kappa,\lambda}(\omega) = \pi \int_{-\infty}^{+\infty} \frac{dk_x}{2\pi} \int_{-\infty}^{+\infty} \frac{dk_y}{2\pi} \mathcal{F}_{\lambda,\lambda}^{\kappa;jj}(k_x, k_y) \left[-\frac{df[\varepsilon_\kappa^\lambda(k_x, k_y)]}{d\varepsilon_\kappa^\lambda(k_x, k_y)} \right] \delta(\omega), \tag{11}$$

where $\delta(x)$ is the Dirac δ function, $f(x) = \{1 + \exp[(x - \mu)/k_B T]\}^{-1}$ denotes the Fermi distribution function in which k_B is the Boltzmann constant and T represents the temperature, and $\mathcal{F}_{\lambda,\lambda'}^{\kappa;jj}(k_x, k_y)$ is explicitly given as

$$\mathcal{F}_{\lambda,\lambda'}^{\kappa;xx}(k_x, k_y) = \frac{e^2}{2} v_x^2 \left\{ 1 + \lambda\lambda' \frac{v_x^2 k_x^2 - v_y^2 k_y^2}{[\mathcal{Z}(k_x, k_y)]^2} \right\}, \tag{12}$$

$$\mathcal{F}_{\lambda,\lambda'}^{\kappa;yy}(k_x, k_y) = \frac{e^2}{2} v_y^2 \left\{ 2t^2 \delta_{\lambda\lambda'} + 1 - \lambda\lambda' \frac{v_x^2 k_x^2 - v_y^2 k_y^2}{[\mathcal{Z}(k_x, k_y)]^2} + 4\lambda\delta_{\lambda\lambda'} \frac{\kappa t v_y k_y}{\mathcal{Z}(k_x, k_y)} \right\}, \tag{13}$$

with $\delta_{\lambda\lambda'}$ the Kronecker symbol.

For the sake of simplicity, we denote the real part of total LOCs as

$$\mathrm{Re}\sigma_{jj}(\omega) = \mathrm{Re}\sigma_{jj}^{\mathrm{IB}}(\omega) + \mathrm{Re}\sigma_{jj}^{\mathrm{D}}(\omega), \tag{14}$$

where $\mathrm{Re}\sigma_{jj}^{\mathrm{IB}}(\omega)$ and $\mathrm{Re}\sigma_{jj}^{\mathrm{D}}(\omega)$ are recast as

$$\frac{\mathrm{Re}\sigma_{jj}^{\mathrm{IB}}(\omega)}{\sigma_0} = \frac{v_x}{v_y} \Gamma_{xx}^{\mathrm{IB}}(\omega)\delta_{jx} + \frac{v_y}{v_x} \Gamma_{yy}^{\mathrm{IB}}(\omega)\delta_{jy}, \tag{15}$$

$$\frac{\mathrm{Re}\sigma^{\mathrm{D}}_{jj}(\omega)}{\sigma_0} = \frac{v_x}{v_y}\Gamma^{\mathrm{D}}_{xx}(\mu,t,\Lambda)\delta_{jx}\,\delta(\omega) + \frac{v_y}{v_x}\Gamma^{\mathrm{D}}_{yy}(\mu,t,\Lambda)\delta_{jy}\,\delta(\omega). \tag{16}$$

In these notations, $\sigma_0 = e^2/4\hbar$ (we temporarily restore $\hbar$ for explicitness), and $\Gamma^{\mathrm{IB}}_{jj}(\omega)$ and $\Gamma^{\mathrm{D}}_{jj}(\mu,t,\Lambda)$ are introduced for convenience with $j = x, y$, whose explicit definitions are independent of the ratio v_x/v_y (see Appendix B for details). The relation between the LOCs and the ratio of Fermi velocities v_x/v_y has also been reported in Refs. [28,30]. Obviously, the only difference between the *isotropic* case ($v_x = v_y$) and the *anisotropic* case ($v_x \neq v_y$) is the magnitude of the LOCs. It is emphasized that $\sigma_0\frac{v_x}{v_y}\Gamma^{\mathrm{D}}_{xx}(\mu,t,\Lambda)$ and $\sigma_0\frac{v_y}{v_x}\Gamma^{\mathrm{D}}_{yy}(\mu,t,\Lambda)$ refer to the Drude weights for $\mathrm{Re}\sigma^{\mathrm{D}}_{xx}$ and $\mathrm{Re}\sigma^{\mathrm{D}}_{yy}$, respectively.

In the next, we will analytically calculate the interband and intraband LOCs by assuming zero temperature $T = 0$ such that the Fermi distribution function $f(x)$ can be replaced by the Heaviside step function $\Theta[\mu - x]$. To better analyze the physics of interband LOCs, we also evaluate the JDOS defined by

$$\mathcal{J}(\omega) = g_s \sum_{\kappa=\pm1} \mathcal{J}_\kappa(\omega), \tag{17}$$

where

$$\mathcal{J}_\kappa(\omega) = \int \frac{d^2\boldsymbol{k}}{(2\pi)^2}\delta[\omega - 2\mathcal{Z}(k_x,k_y)]\{\Theta[\mu - \varepsilon^-_\kappa(k_x,k_y)] - \Theta[\mu - \varepsilon^+_\kappa(k_x,k_y)]\}. \tag{18}$$

The detailed analytical calculations of LOCs and JDOS are found in Appendices B and C.

III. INTERBAND CONDUCTIVITY AND JDOS

In this section, the analytical results of the interband LOC and JDOS are listed for different tilts. Firstly, the LOCs in the undoped case ($\mu = 0$) are completely contributed by the interband transition, which are given as

$$\Gamma^{\mathrm{IB}}_{xx}(\omega) = \begin{cases} 1, & 0 \leqslant t \leqslant 1 \\ G_-\left(\frac{1}{t}\right) - G_-\left(-\frac{1}{t}\right), & t > 1 \end{cases} \tag{19}$$

and

$$\Gamma^{\mathrm{IB}}_{yy}(\omega) = \begin{cases} 1, & 0 \leqslant t \leqslant 1 \\ G_+\left(\frac{1}{t}\right) - G_+\left(-\frac{1}{t}\right), & t > 1, \end{cases} \tag{20}$$

where two auxiliary functions

$$G_\pm(x) = \frac{1}{2} + \frac{\arcsin x}{\pi} \pm \frac{x\sqrt{1-x^2}}{\pi} \tag{21}$$

are introduced for simplicity. It is interesting to note that in the undoped case the LOCs are constant in frequency. Specifically, these constant conductivities depend on the tilt parameter only in the type-II Dirac materials, but are independent of the tilt parameter in both the type-I and type-III Dirac materials.

Hereafter, we focus on the interband LOCs in the doped case for different tilts. In the untilted case ($t = 0$), we recover the result of the ordinary Dirac cone and get

$$\Gamma^{\mathrm{IB}}_{xx}(\omega) = \Gamma^{\mathrm{IB}}_{yy}(\omega) = \Theta(\omega - 2\mu),$$

which are consistent with Refs. [84–88]. The corresponding JDOS is given as

$$\frac{\mathcal{J}(\omega)}{\mathcal{J}_0\omega} = \begin{cases} 0, & 0 < \omega < 2\mu \\ 1, & \omega \geqslant 2\mu, \end{cases} \tag{22}$$

with $\mathcal{J}_0 = \frac{1}{2\pi v_x v_y}$.

When the Dirac cone is tilted ($t > 0$), we introduce three compacted notations

$$\xi_\pm = \frac{2\mu \pm \omega}{\omega}\frac{\Theta(t)}{t},$$
$$\omega_1(t) = 2\mu\frac{\Theta(t)}{1+t},$$
$$\omega_2(t) = 2\mu\Theta(t)\left[\frac{\Theta(1-t)}{1-t} + \frac{\Theta(t-1)}{t-1}\right],$$

in order to simplify our results. The reason that we still used the step function $\Theta(t)$ in these notations is just to emphasize the constraint $t > 0$ without the need of referring to the context. In the subsequent three subsections, we list the analytical expressions of the interband conductivity for the type-I, type-II, and type-III Dirac materials in sequence. In the fourth subsection, we express $\Gamma^{\mathrm{IB}}_{xx}(\omega)$ and $\Gamma^{\mathrm{IB}}_{yy}(\omega)$ in terms of the corresponding JDOS.

A. For type-I Dirac materials

For the type-I phase ($0 < t < 1$), the interband conductivities can be expressed by

$$\Gamma^{\mathrm{IB}}_{xx}(\omega) = \begin{cases} 0, & 0 < \omega < \omega_1(t) \\ 1 - G_-(\xi_-), & \omega_1(t) \leqslant \omega < \omega_2(t) \\ 1, & \omega \geqslant \omega_2(t) \end{cases} \tag{23}$$

and

$$\Gamma^{\mathrm{IB}}_{yy}(\omega) = \begin{cases} 0, & 0 < \omega < \omega_1(t) \\ 1 - G_+(\xi_-), & \omega_1(t) \leqslant \omega < \omega_2(t) \\ 1, & \omega \geqslant \omega_2(t), \end{cases} \tag{24}$$

where $\xi_\pm = (2\mu \pm \omega)/t\omega$. The corresponding JDOS $\mathcal{J}(\omega)$ is given by

$$\frac{\mathcal{J}(\omega)}{\mathcal{J}_0\omega} = \begin{cases} 0, & 0 < \omega < \omega_1(t) \\ \frac{\arccos\xi_-}{\pi}, & \omega_1(t) \leqslant \omega < \omega_2(t) \\ 1, & \omega \geqslant \omega_2(t). \end{cases} \tag{25}$$

It is noted that there are two tilt-dependent critical boundaries at $\omega = \omega_1(t) = 2\mu/(1+t)$ and $\omega = \omega_2(t) = 2\mu/(1-t)$ in the interband LOCs, which are also confirmed by the JDOS. In addition, $\frac{d\Gamma^{\mathrm{IB}}_{yy}(\omega)}{d\omega}$ is continuous at $\omega = \omega_1(t)$ and $\omega = \omega_2(t)$, while $\frac{d\Gamma^{\mathrm{IB}}_{xx}(\omega)}{d\omega}$ is discontinuous thereabouts. These expressions agree exactly with the analytical results in Ref. [30]. After substituting $v_x = 0.86v_F$, $v_y = 0.69v_F$, and $v_t = 0.32v_F$ with $v_F = 10^6$ m/s into Eq. (15), these expressions give rise to the numerical results reported in Ref. [27]. Furthermore, these results are also valid in the

untilted limit ($t \to 0^+$) and/or undoped case ($\mu = 0$). In the regime of large photon energy where $\omega \gg \mathrm{Max}\{\omega_2(t), 2\mu\}$ which leads to $\xi_\pm = \pm 1/t$, these interband conductivities approach the asymptotic background values $\mathrm{Re}\sigma_{xx}^{\mathrm{asymp}}(\omega) = \frac{v_x}{v_y}\sigma_0$ and $\mathrm{Re}\sigma_{yy}^{\mathrm{asymp}}(\omega) = \frac{v_y}{v_x}\sigma_0$, which satisfy $\mathrm{Re}\sigma_{xx}^{\mathrm{asymp}}(\omega) \times \mathrm{Re}\sigma_{yy}^{\mathrm{asymp}}(\omega) = \sigma_0^2$. It is evident that the asymptotic background values and their product are independent of the tilt parameter, which is the same as reported in Ref. [30].

B. For type-II Dirac materials

For the type-II phase ($t > 1$), the interband conductivities take the form

$$\Gamma_{xx}^{\mathrm{IB}}(\omega) = \begin{cases} 0, & 0 < \omega < \omega_1(t) \\ 1 - G_-(\xi_-), & \omega_1(t) \leqslant \omega < \omega_2(t) \\ \sum_{\chi=\pm1} \chi G_-(\xi_\chi), & \omega \geqslant \omega_2(t) \end{cases} \tag{26}$$

and

$$\Gamma_{yy}^{\mathrm{IB}}(\omega) = \begin{cases} 0, & 0 < \omega < \omega_1(t) \\ 1 - G_+(\xi_-), & \omega_1(t) \leqslant \omega < \omega_2(t) \\ \sum_{\chi=\pm1} \chi G_+(\xi_\chi), & \omega \geqslant \omega_2(t), \end{cases} \tag{27}$$

where $\xi_\pm = (2\mu \pm \omega)/t\omega$. The corresponding JDOS $\mathcal{J}(\omega)$ reads

$$\frac{\mathcal{J}(\omega)}{\mathcal{J}_0\omega} = \begin{cases} 0, & 0 < \omega < \omega_1(t) \\ \frac{\arccos\xi_-}{\pi}, & \omega_1(t) \leqslant \omega < \omega_2(t) \\ \frac{\arcsin\xi_+ - \arcsin\xi_-}{\pi}, & \omega \geqslant \omega_2(t). \end{cases} \tag{28}$$

There are also two tilt-dependent critical boundaries at $\omega = \omega_1(t) = 2\mu/(t+1)$ and $\omega = \omega_2(t) = 2\mu/(t-1)$ in the interband LOCs, which are also confirmed by the JDOS. Note that in this case, $\frac{d\Gamma_{yy}^{\mathrm{IB}}(\omega)}{d\omega}$ is continuous, while $\frac{d\Gamma_{xx}^{\mathrm{IB}}(\omega)}{d\omega}$ is discontinuous at these two tilt-dependent critical boundaries. In the regime of large photon energy where $\omega \gg \mathrm{Max}\{\omega_2(t), 2\mu\}$ which leads to $\xi_\pm = \pm 1/t$, the asymptotic background values can be obtained as

$$\mathrm{Re}\sigma_{xx}^{\mathrm{asymp}}(t) = \frac{v_x}{v_y}\sigma_0\left[G_-\left(\frac{1}{t}\right) - G_-\left(-\frac{1}{t}\right)\right], \tag{29}$$

$$\mathrm{Re}\sigma_{yy}^{\mathrm{asymp}}(t) = \frac{v_y}{v_x}\sigma_0\left[G_+\left(\frac{1}{t}\right) - G_+\left(-\frac{1}{t}\right)\right], \tag{30}$$

which is a straightforward consequence of the LOCs in the undoped case. In addition, they satisfy

$$\mathrm{Re}\sigma_{xx}^{\mathrm{asymp}}(t) \times \mathrm{Re}\sigma_{yy}^{\mathrm{asymp}}(t) = \frac{4}{\pi^2}\left[\frac{1}{t^4} - \frac{1}{t^2} + \arcsin^2\left(\frac{1}{t}\right)\right]\sigma_0^2, \tag{31}$$

which, different from that in the type-I phase, is tilt dependent.

C. For type-III Dirac materials

For the type-III phase ($t = 1$), the interband conductivities are given as

$$\Gamma_{xx}^{\mathrm{IB}}(\omega) = \begin{cases} 0, & 0 < \omega < \mu \\ 1 - G_-(\xi_-), & \omega \geqslant \mu \end{cases} \tag{32}$$

and

$$\Gamma_{yy}^{\mathrm{IB}}(\omega) = \begin{cases} 0, & 0 < \omega < \mu \\ 1 - G_+(\xi_-), & \omega \geqslant \mu, \end{cases} \tag{33}$$

where $\xi_\pm = (2\mu \pm \omega)/\omega$. The corresponding JDOS $\mathcal{J}(\omega)$ is given by

$$\frac{\mathcal{J}(\omega)}{\mathcal{J}_0\omega} = \begin{cases} 0, & 0 < \omega < \mu \\ \frac{\arccos\xi_-}{\pi}, & \omega \geqslant \mu. \end{cases} \tag{34}$$

It is remarked that there is only one finite critical boundary at $\omega = \mu = \omega_1(1)$ in the interband LOCs, which is also confirmed by the corresponding JDOS. Moreover, around this critical boundary, $\frac{d\Gamma_{yy}^{\mathrm{IB}}(\omega)}{d\omega}$ is continuous, while $\frac{d\Gamma_{xx}^{\mathrm{IB}}(\omega)}{d\omega}$ is not. In the regime of large photon energy where $\omega \gg 2\mu$, these interband conductivities approach to the asymptotic background values $\mathrm{Re}\sigma_{xx}^{\mathrm{asymp}}(\omega) = \frac{v_x}{v_y}\sigma_0$ and $\mathrm{Re}\sigma_{yy}^{\mathrm{asymp}}(\omega) = \frac{v_y}{v_x}\sigma_0$. The results for the interband LOCs, the JDOS, the asymptotic background values, and their product $\mathrm{Re}\sigma_{xx}^{\mathrm{asymp}}(\omega) \times \mathrm{Re}\sigma_{yy}^{\mathrm{asymp}}(\omega)$ can also be obtained from that of type-I phase in the limit $t \to 1^-$ or from that of type-II phase in the limit $t \to 1^+$. As a consequence, the interband conductivities are continuous when the tilt parameter changes from $t < 1$ to $t > 1$ through $t = 1$.

D. Relation between $\Gamma_{jj}^{\mathrm{IB}}(\omega)$ and $\mathcal{J}(\omega)$

In this section, we express $\Gamma_{xx}^{\mathrm{IB}}(\omega)$ and $\Gamma_{yy}^{\mathrm{IB}}(\omega)$ alternatively in terms of the corresponding JDOS as

$$\Gamma_{xx}^{\mathrm{IB}}(\omega) = \frac{\mathcal{J}(\omega)}{\mathcal{J}_0\omega} - \mathcal{L}(\omega), \tag{35}$$

$$\Gamma_{yy}^{\mathrm{IB}}(\omega) = \frac{\mathcal{J}(\omega)}{\mathcal{J}_0\omega} + \mathcal{L}(\omega). \tag{36}$$

From these two relations, it can be found that $\Gamma_{xx}^{\mathrm{IB}}(\omega)$ and $\Gamma_{yy}^{\mathrm{IB}}(\omega)$ depend on JDOS in terms of $\frac{\mathcal{J}(\omega)}{\mathcal{J}_0\omega}$ rather than $\mathcal{J}(\omega)$, and on the auxiliary function $\mathcal{L}(\omega)$ in the opposite way. The auxiliary function $\mathcal{L}(\omega)$ is explicitly written as

$$\mathcal{L}(\omega) = g_s \sum_{\kappa=\pm1} \mathcal{L}_\kappa(\omega), \tag{37}$$

where

$$\mathcal{L}_\kappa(\omega) = 2\pi v_x v_y \times \int \frac{d^2\boldsymbol{k}}{(2\pi)^2} \frac{v_x^2 k_x^2 - v_y^2 k_y^2}{[\mathcal{Z}(k_x, k_y)]^2} \delta[\omega - 2\mathcal{Z}(k_x, k_y)] \times \frac{\Theta[\mu - \varepsilon_\kappa^-(k_x, k_y)] - \Theta[\mu - \varepsilon_\kappa^+(k_x, k_y)]}{\omega}. \tag{38}$$

It is emphasized that in the untilted phase ($t = 0$), we have $\mathcal{L}_\kappa(\omega) = 0$ after taking the symmetry of integration into account, and hence the auxiliary function $\mathcal{L}(\omega) = 0$. As a direct result, the dimensionless function $\Gamma_{jj}^{\mathrm{IB}}(\omega)$ can be written as $\Gamma_{xx}^{\mathrm{IB}}(\omega) = \Gamma_{yy}^{\mathrm{IB}}(\omega) = \frac{\mathcal{J}(\omega)}{\mathcal{J}_0\omega}$. However, in the tilted phase ($t > 0$), the auxiliary function $\mathcal{L}(\omega)$ does not always vanish along other directions. As a direct consequence, $\Gamma_{xx}^{\mathrm{IB}}(\omega) \neq \Gamma_{yy}^{\mathrm{IB}}(\omega)$, which implies that $\mathcal{L}(\omega)$ can characterize the anisotropy between $\Gamma_{xx}^{\mathrm{IB}}(\omega)$ and $\Gamma_{yy}^{\mathrm{IB}}(\omega)$ originating from the tilting of Dirac bands.

After some straightforward algebra (see Appendix D for details), we arrive at the explicit expressions of $\mathcal{L}(\omega)$ for the

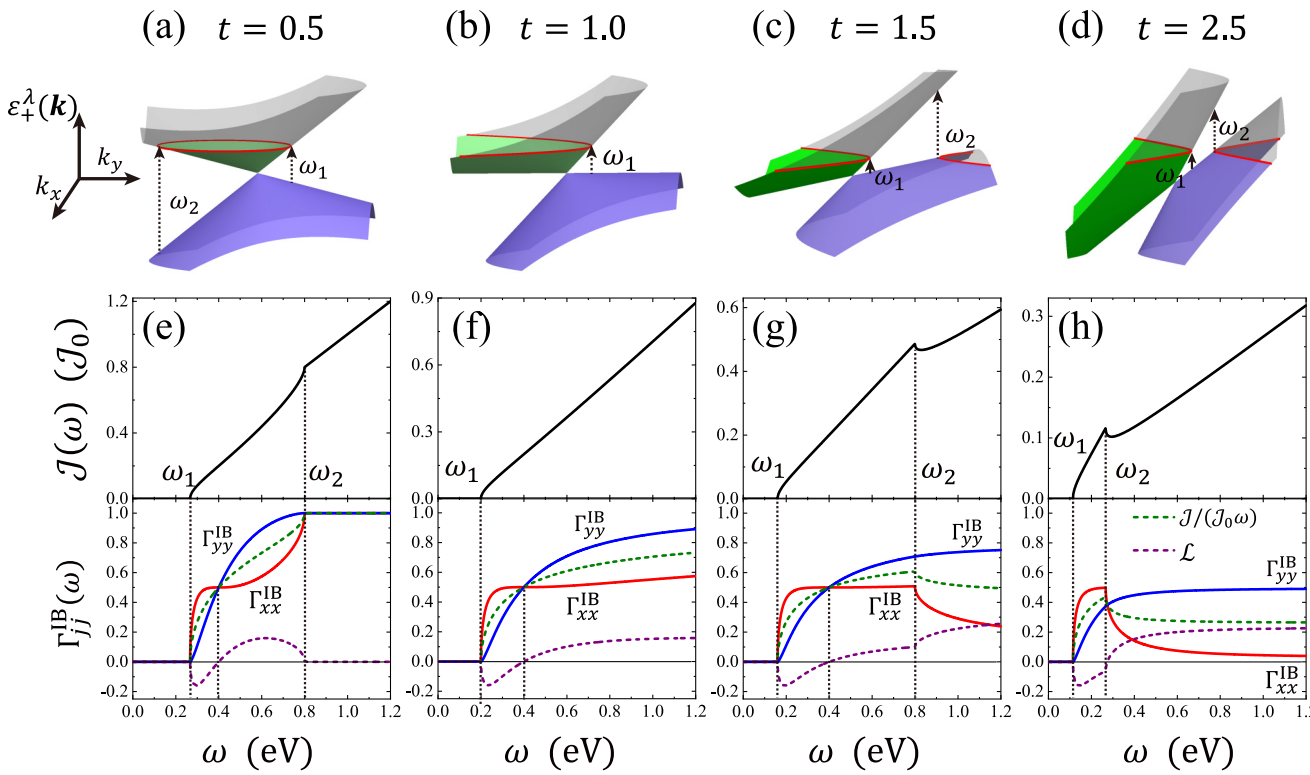

FIG. 2. Schematic interband transitions, the JDOS $\mathcal{J}(\omega)$, and the relation among $\Gamma_{jj}^{\mathrm{IB}}(\omega)$, $\mathcal{J}(\omega)$, and $\mathcal{L}(\omega)$. In panels (a), (c), and (d), two Van Hove singularities appear at $\omega = \omega_1(t)$ and $\omega = \omega_2(t)$ in the type-I and type-II phases, but in panel (b), only one Van Hove singularity exists at $\omega = \omega_1(t)$ in the type-III phase. In the top panel of (e)–(h), the JDOS $\mathcal{J}(\omega)$ and the corresponding Van Hove singularities are shown, while in the bottom panel of (e)–(h), $\Gamma_{jj}^{\mathrm{IB}}(\omega)$ and the relation with $\mathcal{J}(\omega)$ and $\mathcal{L}(\omega)$ are presented, respectively.

type-I phase ($0 < t < 1$) as

$$\mathcal{L}(\omega) = \begin{cases} 0, & 0 < \omega < \omega_1(t) \\ \frac{-\xi_-\sqrt{1-\xi_-^2}}{\pi}, & \omega_1(t) \leqslant \omega < \omega_2(t) \\ 0, & \omega \geqslant \omega_2(t), \end{cases} \tag{39}$$

for the type-II phase ($t > 1$) as

$$\mathcal{L}(\omega) = \begin{cases} 0, & 0 < \omega < \omega_1(t) \\ \frac{-\xi_-\sqrt{1-\xi_-^2}}{\pi}, & \omega_1(t) \leqslant \omega < \omega_2(t) \\ \frac{\xi_+\sqrt{1-\xi_+^2}-\xi_-\sqrt{1-\xi_-^2}}{\pi}, & \omega \geqslant \omega_2(t), \end{cases} \tag{40}$$

and for the type-III phase ($t = 1$) as

$$\mathcal{L}(\omega) = \begin{cases} 0, & 0 < \omega < \mu \\ \frac{-\xi_-\sqrt{1-\xi_-^2}}{\pi}, & \omega \geqslant \mu. \end{cases} \tag{41}$$

IV. RESULTS FOR THE INTERBAND CONDUCTIVITY

Utilizing the analytical expressions listed in the previous section, we plot the interband transitions, JDOS, and LOCs, in Fig. 2. We at first present four general findings. First, the interband conductivities are anisotropic, due to the band tilting and Pauli blocking. Second, when $t \neq 0$ and $t \neq 1$, the JDOS possesses two Van Hove singularities at $\omega = \omega_1(t)$ and $\omega = \omega_2(t)$, leading to two critical boundaries in the LOC. Third, in the region $0 < \omega < \omega_1(t)$, the real part of LOCs always vanish, namely, $\Gamma_{jj}^{\mathrm{IB}}(\omega) \equiv 0$. Fourth, the results are valid for both the *n*-doped and *p*-doped cases.

For the type-I phase ($0 < t < 1$), it can be seen from Fig. 2(e) that in the region $\omega_1(t) \leqslant \omega < \omega_2(t)$, $\Gamma_{jj}^{\mathrm{IB}}(\omega)$ increases monotonically from zero at $\omega = \omega_1(t)$ to one at $\omega = \omega_2(t)$, and that $\Gamma_{jj}^{\mathrm{IB}}(\omega) \equiv 1$ when $\omega \geqslant \omega_2(t)$. By contrast, for the type-II phase ($t > 1$), as shown in Figs. 2(g) and 2(h), $\Gamma_{jj}^{\mathrm{IB}}(\omega)$ increases monotonically from zero at $\omega = \omega_1(t)$ to the corresponding critical value at $\omega = \omega_2(t)$. When $\omega \geqslant \omega_2(t)$, however, $\Gamma_{xx}^{\mathrm{IB}}(\omega)$ drops dramatically in magnitude whereas $\Gamma_{yy}^{\mathrm{IB}}(\omega)$ becomes larger smoothly with the increasing of photon energy. This difference results from the competition between $\frac{\mathcal{J}(\omega)}{\mathcal{J}_0\omega}$ and $\mathcal{L}(\omega)$. Explicitly, when $\omega \geqslant \omega_2(t)$, $\frac{\mathcal{J}(\omega)}{\mathcal{J}_0\omega}$ is identically equal to one in the type-I phase whereas $\frac{\mathcal{J}(\omega)}{\mathcal{J}_0\omega}$ decreases monotonously in the type-II phase, the latter of which originates from the dip in JDOS. On the other hand, in this region $\mathcal{L}(\omega)$ vanishes for the type-I phase whereas $\mathcal{L}(\omega)$ increases monotonously with ω for the type-II phase. In the region $\omega > \omega_2(t)$, the relative changes of $\frac{\mathcal{J}(\omega)}{\mathcal{J}_0\omega}$ and $\mathcal{L}(\omega)$ determine the dramatically different behaviors of $\Gamma_{xx}^{\mathrm{IB}}(\omega)$ and $\Gamma_{yy}^{\mathrm{IB}}(\omega)$ in the type-I and type-II phases, leading to a consequence that $\Gamma_{xx}^{\mathrm{IB}}(\omega) = \Gamma_{yy}^{\mathrm{IB}}(\omega)$ in the type-I phase while $\Gamma_{xx}^{\mathrm{IB}}(\omega) \neq \Gamma_{yy}^{\mathrm{IB}}(\omega)$ in the type-II phase, as shown in the bottom panels of Fig. 2. Specifically, for the type-III phase ($t = 1$), the JDOS exhibits one Van Hove singularity at $\omega = \omega_1(t) = \mu$ and one Van Hove singularity at $\omega = \omega_2(t) = \infty$. As a result, there is only one critical boundary at finite frequency in the LOCs, as shown in Fig. 2(f). For the untilted case ($t = 0$), the

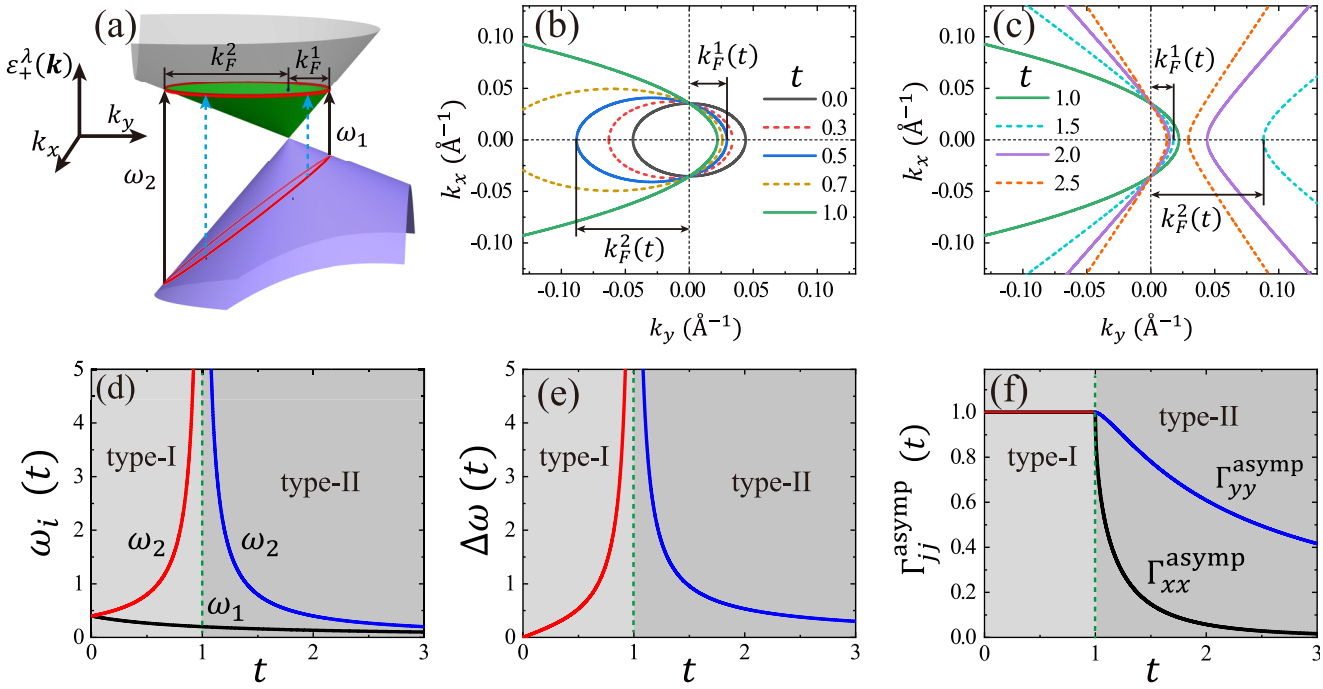

FIG. 3. Schematic diagram of interband transition, the dependence of two critical boundaries $\omega = \omega_i(t)$, their separation $\Delta\omega(t)$, and the asymptotic background values $\Gamma_{jj}^{\text{asymp}}(t)$ on the tilt parameter t. In panel (a), the interband transitions and two critical boundaries are schematically shown, where two critical boundaries $\omega = \omega_1(t) = 2v_y k_F^1(t)$ and $\omega = \omega_2(t) = 2v_y k_F^2(t)$ and the corresponding Fermi wave vectors $k_F^1(t) = \frac{\mu}{(1+t)v_y}$ and $k_F^2(t) = \frac{\mu}{|1-t|v_y}$ are labeled. The Fermi surfaces projected onto the k_x-k_y plane are shown in panels (b) and (c). Two Fermi wave vectors $k_F^1(t)$ and $k_F^2(t)$ can reflect the corresponding changes in $\omega = \omega_1(t)$ and $\omega = \omega_2(t)$ with respect to t. As t increases, $k_F^1(t)$ always decreases. In comparison, $k_F^2(t)$ becomes larger when $0 < t < 1$ but becomes smaller for $t > 1$. In panel (d), the first critical boundary at $\omega = \omega_1(t)$ is represented by the black line in both the type-I and type-II phases, while the second critical boundary at $\omega = \omega_2(t)$ is denoted either by the red line in the type-I phase or by the blue line in the type-II phase. These are in exact agreement with the trend of $\omega_1(t)$ and $\omega_2(t)$ in panels (a)–(c). The separation between two critical boundaries $\Delta\omega(t)$ is shown in (e): type-I phase (red line) and type-II phase (blue line). The dependence of asymptotic background values $\Gamma_{jj}^{\text{asymp}}(t)$ on the tilt parameter t are shown in (f): $\Gamma_{xx}^{\text{asymp}}(t) = \Gamma_{yy}^{\text{asymp}}(t) = 1$ in the type-I phase but $\Gamma_{xx}^{\text{asymp}}(t) < \Gamma_{yy}^{\text{asymp}}(t) < 1$ in the type-II phase.

JDOS exhibits only one Van Hove singularity at $\omega = 2\mu$, so the LOC behaves as a step function.

Interestingly, when $0 < t \leqslant 2$,

$$\Gamma_{xx}^{\text{IB}}(2\mu) = \Gamma_{yy}^{\text{IB}}(2\mu) = \tfrac{1}{2}, \tag{42}$$

as a consequence of $\mathcal{L}(2\mu) = 0$, and when $t \geqslant 2$,

$$\Gamma_{xx}^{\text{IB}}(2\mu\sqrt{2/(t^2-2)}) = \Gamma_{yy}^{\text{IB}}(2\mu\sqrt{2/(t^2-2)}) = \frac{\arcsin[\zeta_+(t)] - \arcsin[\zeta_-(t)]}{\pi} \tag{43}$$

with $\zeta_\pm(t) = \frac{1}{t}(\sqrt{\frac{t^2-2}{2}} \pm 1)$.

The tilt parameter t and the chemical potential μ can be extracted from optical experiments by measuring two critical boundaries at $\omega = \omega_1(t)$ and $\omega = \omega_2(t)$. As shown in Fig. 3, the first critical boundary $\omega = \omega_1(t)$ decreases monotonically with the increasing of t no matter in the type-I phase ($0 < t < 1$) or type-II phase ($t > 1$); however, the second critical boundary $\omega = \omega_2(t)$ increases in the type-I phase ($0 < t < 1$) and decreases in the type-II phase ($t > 1$) as t increases. Explicitly, the tilt parameter t satisfies the relation

$$t = \frac{\omega_2(t) - \omega_1(t)}{\omega_2(t) + \omega_1(t)}. \tag{44}$$

Combined with the separation between two critical boundaries

$$\Delta\omega(t) = \omega_2(t) - \omega_1(t) = \begin{cases} \frac{4\mu t}{1-t^2}, & 0 < t < 1 \\ \frac{4\mu}{t^2-1}, & t > 1, \end{cases} \tag{45}$$

one can further determine the chemical potential μ. Interestingly, it is shown in Fig. 3(e) that with increasing the tilt parameter t this separation becomes larger in the type-I phase ($0 < t < 1$) whereas smaller in the type-II phase ($t > 1$). In experiments, the positions of these two critical boundaries and their separation can also be used to determine whether the Lifshitz transition occurs and which phase the Dirac materials belong to.

In addition, the asymptotic background values $\Gamma_{jj}^{\text{asymp}}(t)$ behave dramatically different in the type-I phase and type-II phase, as shown in Fig. 3(f). For the type-I phase, $\Gamma_{xx}^{\text{asymp}}(t)$ and $\Gamma_{yy}^{\text{asymp}}(t)$ are always identically equal to 1. By contrast, for the type-II phase, $\Gamma_{xx}^{\text{asymp}}(t)$ and $\Gamma_{yy}^{\text{asymp}}(t)$ decrease with t and always satisfy the relation $\Gamma_{xx}^{\text{asymp}}(t) < \Gamma_{yy}^{\text{asymp}}(t) < 1$. In addition, for the type-III phase, the asymptotic background values satisfy $\Gamma_{xx}^{\text{asymp}}(t=1) = \Gamma_{yy}^{\text{asymp}}(t=1) = 1$. Hence, the asymptotic background values $\Gamma_{jj}^{\text{asymp}}(t)$ can also be taken as fingerprints of type-I phase and type-II phase.

V. DRUDE CONDUCTIVITY

In this section, we turn to the Drude conductivities contributed by the intraband transition around the Fermi surface. At zero temperature, the derivative of the Fermi distribution function in Eq. (11) can be replaced by $\delta[\mu-\varepsilon_\kappa^\lambda(k_x,k_y)]$. In the untilted case ($t=0$), we recover the result of the ordinary Dirac cone as

$$\Gamma_{xx}^{\mathrm{D}}(\mu,t,\Lambda)=\Gamma_{yy}^{\mathrm{D}}(\mu,t,\Lambda)=4\mu,$$

which is exactly the same as that in Ref. [84]. For the type-I phase ($0<t<1$), we arrive at

$$\Gamma_{xx}^{\mathrm{D}}(\mu,t,\Lambda)=8\mu\frac{1-\sqrt{1-t^2}}{t^2\sqrt{1-t^2}}, \tag{46}$$

$$\Gamma_{yy}^{\mathrm{D}}(\mu,t,\Lambda)=8\mu\frac{1-\sqrt{1-t^2}}{t^2}. \tag{47}$$

Four remarks for the type-I phase are in order here. First, these results are also valid in the untilted limit ($t\to 0^+$). Second, in the critical-tilted limit ($t\to 1^-$), $\Gamma_{yy}^{\mathrm{D}}(\mu,t,\Lambda)=8\mu$ but $\Gamma_{xx}^{\mathrm{D}}(\mu,t,\Lambda)$ is divergent. Third, the ratio $\Gamma_{xx}^{\mathrm{D}}(\mu,t,\Lambda)/\Gamma_{yy}^{\mathrm{D}}(\mu,t,\Lambda)$ is always $1/\sqrt{1-t^2}$. Fourth, $\Gamma_{jj}^{\mathrm{D}}(\mu,t,\Lambda)$ are always convergent when $0<t<1$, and yield the numerical results of Drude weight in Ref. [27], namely, $N_1=4.686$ and $N_2=2.673$ after applying the parameters of 8-*Pmmn* borophene ($v_x=0.86v_F$, $v_y=0.69v_F$, and $v_t=0.32v_F$ with $v_F=10^6$ m/s). The detailed evaluation can be found in Appendix B.

For the type-II and type-III phases ($t\geqslant 1$), we introduce a momentum cutoff Λ to account for the limitation of integration interval, which is a measure of the density of states due to the electron and hole pockets [79]. For the type-II phase ($t>1$), the Drude contributions are given by

$$\Gamma_{xx}^{\mathrm{D}}(\mu,t,\Lambda)=\frac{8\mu}{\pi}\left[A(\mu,t,\Lambda)\frac{2\Lambda}{\mu}+\frac{B(\mu,t,\Lambda)}{\sqrt{t^2-1}}-C(\mu,t,\Lambda)\right], \tag{48}$$

$$\Gamma_{yy}^{\mathrm{D}}(\mu,t,\Lambda)=\frac{8\mu}{\pi}\left[(t^2-1)A(\mu,t,\Lambda)\frac{2\Lambda}{\mu}+\sqrt{t^2-1}B(\mu,t,\Lambda)+C(\mu,t,\Lambda)\right], \tag{49}$$

where

$$A(\mu,t,\Lambda)=\sum_{\chi=\pm}\frac{1}{2t}\sqrt{1-\left(\frac{\mu-\chi\Lambda}{t\Lambda}\right)^2},$$

$$B(\mu,t,\Lambda)=\frac{1}{t^2}\ln\frac{t^2+\frac{\mu-\Lambda}{\Lambda}+\sqrt{t^2-1}\sqrt{t^2-(\frac{\mu-\Lambda}{\Lambda})^2}}{t^2-\frac{\mu+\Lambda}{\Lambda}+\sqrt{t^2-1}\sqrt{t^2-(\frac{\mu+\Lambda}{\Lambda})^2}},$$

$$C(\mu,t,\Lambda)=\sum_{\chi=\pm}\frac{1}{t^2}\arccos\frac{\mu-\chi\Lambda}{t\Lambda}. \tag{50}$$

Keeping up to $O(1)$ of Λ, we have the approximate expressions

$$\Gamma_{xx}^{\mathrm{D}}(\mu,t,\Lambda)=8\mu\left[\frac{\sqrt{t^2-1}}{\pi t^2}\frac{2\Lambda}{\mu}-\frac{1}{t^2}\right], \tag{51}$$

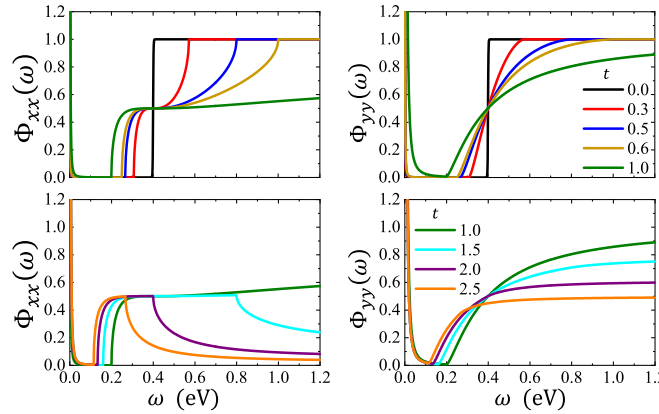

FIG. 4. The dependence of $\Phi_{xx}(\omega)$ and $\Phi_{yy}(\omega)$ on the tilt parameter. $\Phi_{xx}(\omega)$ and $\Phi_{yy}(\omega)$ are plotted by utilizing the relations given in Eqs. (57)–(59). In the numerical calculation, the chemical potential is set to $\mu=0.2$ eV.

$$\Gamma_{yy}^{\mathrm{D}}(\mu,t,\Lambda)=8\mu\left[\frac{\sqrt{(t^2-1)^3}}{\pi t^2}\frac{2\Lambda}{\mu}+\frac{1}{t^2}\right], \tag{52}$$

which indicate that both $\Gamma_{xx}^{\mathrm{D}}(\mu,t,\Lambda)$ and $\Gamma_{yy}^{\mathrm{D}}(\mu,t,\Lambda)$ are divergent when the cutoff Λ is taken to be infinity.

For the type-III phase ($t=1$), the intraband contributions read

$$\Gamma_{xx}^{\mathrm{D}}(\mu,t,\Lambda)=\frac{16\mu}{\pi}\left[\sqrt{\frac{2\Lambda-\mu}{\mu}}-\arccos\sqrt{\frac{\mu}{2\Lambda}}\right], \tag{53}$$

$$\Gamma_{yy}^{\mathrm{D}}(\mu,t,\Lambda)=\frac{8\mu}{\pi}\arccos\left(\frac{\mu-\Lambda}{\Lambda}\right), \tag{54}$$

which in the limit $\Lambda\to\infty$ reduce to be

$$\Gamma_{xx}^{\mathrm{D}}(\mu,t,\Lambda)=8\mu\left[\frac{2}{\pi}\sqrt{\frac{2\Lambda}{\mu}}-1\right], \tag{55}$$

$$\Gamma_{yy}^{\mathrm{D}}(\mu,t,\Lambda)=8\mu, \tag{56}$$

indicating that $\Gamma_{xx}^{\mathrm{D}}(\mu,t,\Lambda)$ is divergent but $\Gamma_{yy}^{\mathrm{D}}(\mu,t,\Lambda)$ is convergent. By further analyzing $\Gamma_{xx}^{\mathrm{D}}(\mu,t,\Lambda)$ and $\Gamma_{yy}^{\mathrm{D}}(\mu,t,\Lambda)$ around $t=1$, it can be seen that when the tilted Dirac band undergoes a Lifshitz transition from the type-I phase to the type-II phase, the Drude contribution $\Gamma_{yy}^{\mathrm{D}}(\mu,t,\Lambda)$ is continuous, whereas $\Gamma_{xx}^{\mathrm{D}}(\mu,t,\Lambda)$ changes from convergent to divergent.

For convenience, we plot the dependence of the real part of LOCs on the tilt parameter t in Fig. 4 after introducing the relation

$$\frac{\mathrm{Re}\sigma_{jj}(\omega)}{\sigma_0}=\frac{v_x}{v_y}\Phi_{xx}(\omega)\delta_{jx}+\frac{v_y}{v_x}\Phi_{yy}(\omega)\delta_{jy}, \tag{57}$$

with

$$\Phi_{xx}(\omega)=\Gamma_{xx}^{\mathrm{IB}}(\omega)+\Gamma_{xx}^{\mathrm{D}}(\mu,t,\Lambda)\delta(\omega), \tag{58}$$

$$\Phi_{yy}(\omega)=\Gamma_{yy}^{\mathrm{IB}}(\omega)+\Gamma_{yy}^{\mathrm{D}}(\mu,t,\Lambda)\delta(\omega), \tag{59}$$

and utilizing the analytical expressions listed in Secs. III and V. For numerical evaluation, we replace the Dirac δ function in the Drude conductivity with Lorentzians according to

$\delta(x) \to (\eta/\pi)/(x^2+\eta^2)$ with $\eta \to 0^+$. Note that all of the analytical results are independently confirmed by the direct numerical evaluation.

VI. SUMMARY AND CONCLUSIONS

In this work, we theoretically investigated the LOCs in the type-I, type-II, and type-III phases of 2D tilted Dirac energy bands. For the undoped case, the interband LOCs are constants either independent of the tilt parameter in both type-I and type-III phases, or determined by the tilt parameter in the type-II phase. For the doped type-I or type-II phase, the interband LOCs are anisotropic and share two critical boundaries at $\omega = \omega_1(t)$ and $\omega = \omega_2(t)$ confirmed by the JDOS. The tilt parameter t and chemical potential μ can be extracted from optical experiments by measuring the positions of these two peaks and their separation $\Delta\omega(t) = \omega_2(t) - \omega_1(t)$. With increasing the tilt parameter t this separation becomes larger in the type-I phase whereas smaller in the type-II phase. At large photon energy regime, the interband LOCs decay to certain asymptotic values which are exactly the same as that in the undoped case. The Drude conductivity is also anisotropic and sensitive to the structure of the Fermi surface. The relation $\Gamma^{\rm D}_{xx}(\mu,t,\Lambda)/\Gamma^{\rm D}_{yy}(\mu,t,\Lambda) = 1/\sqrt{1-t^2}$ always holds for the type-I phase. In the type-II phase, the Drude conductivity is closely related to the momentum cutoff Λ. When the 2D tilted Dirac band undergoes a Lifshitz transition, $\Gamma^{\rm D}_{yy}(\mu,t,\Lambda)$ is always convergent and continuous, but $\Gamma^{\rm D}_{xx}(\mu,t,\Lambda)$ change from convergent in the type-I phase to divergent in the type-II phase.

Through the shapes, asymptotic background values, critical boundaries, and their separation in the optical conductivity spectrum, such as obtained from the transmissivity and reflectivity measured by optical spectroscopy [86–89], the type of tilted Dirac bands can be determined in very clean samples at extremely low temperature. These quantities can hence be taken as experimental signatures of the Lifshitz transition in the 2D tilted Dirac materials. It is emphasized that the asymptotic background values of LOC do not depend on the chemical potential, temperature, disorder, and band gap [30,79,85–87,90,97]. This can be physically understood by noticing that at large photon energy regime the chemical potential, temperature, disorder, and band gap can be considered to be overwhelmingly small compared to the photon energy ω or the energy $\varepsilon^{\lambda}_{\kappa}(k_x,k_y)$, and hence can be safely neglected in analyzing the asymptotic behavior of LOCs. Consequently, the asymptotic values of LOC are robust against thermal broadening or disorder, although the sharp critical boundaries in the LOCs may not survive. Hence, the physics of Lifshitz transition can still be experimentally realized even in the presence of impurity and/or thermal broadening.

From a comprehensive comparison of LOCs [22,26–28,30,31,84–88,90], it can be concluded that the parameters of specific 2D Dirac materials, such as different anisotropic Fermi velocities and band gaps, do not qualitatively affect the essential physical behaviors. Due to the underlying intrinsic similarities of 2D tilted Dirac bands, the results of this work are expected to be qualitatively valid for a great number of 2D tilted Dirac materials, including α-(BEDT-TTF)$_2$I$_3$, 8-*Pmmn* borophene, α-SnS_2, $TaCoTe_2$, $TaIrTe_4$, and different compounds of $1T'$ transition metal dichalcogenides.

Note added. Recently, a related paper appeared [98], which also examines similar topics, such as the effects of different tilting and anisotropic Fermi velocity on the optical response in 2D tilted Dirac materials and confirms partial findings discussed herein.

ACKNOWLEDGMENTS

We are grateful to Xiang-Hua Kong, Zhi-Qiang Li, and Chen-Yi Zhou for valuable discussions. This work is partially supported by the National Natural Science Foundation of China (NNSFC) under Grant No. 11547200. C.-Y.T. and J.-T.H. acknowledges financial support from the NNSFC under Grants No.11874273 and No. 11874271, respectively. H.-R.C. and H.G. are also supported by the NSERC of Canada and the FQRNT of Quebec (H.G.). We thank the High Performance Computing Centers at Sichuan Normal University, McGill University, and Compute Canada.

APPENDIX A: DEFINITION AND PARTICLE-HOLE SYMMETRY OF LOC AND JDOS

In this Appendix, we give the definition of LOC and JDOS, and prove their particle-hole symmetry.

1. Definition and particle-hole symmetry of LOC

Within linear response theory, the LOC for the photon frequency ω and chemical potential μ is given by

$$\sigma_{jj}(\omega,\mu) = g_s \sum_{\kappa=\pm} \sigma^{\kappa}_{jj}(\omega,\mu), \tag{A1}$$

where

$$\sigma^{\kappa}_{jj}(\omega,\mu) = \frac{i}{\omega}\int_{-\infty}^{+\infty}\frac{dk_x}{2\pi}\int_{-\infty}^{+\infty}\frac{dk_y}{2\pi}\sum_{\lambda=\pm}\sum_{\lambda'=\pm}\mathcal{F}^{\kappa;jj}_{\lambda,\lambda'}(k_x,k_y)\frac{f\left[\varepsilon^{\lambda}_{\kappa}(k_x,k_y),\mu\right]-f\left[\varepsilon^{\lambda'}_{\kappa}(k_x,k_y),\mu\right]}{\omega+\varepsilon^{\lambda}_{\kappa}(k_x,k_y)-\varepsilon^{\lambda'}_{\kappa}(k_x,k_y)+i\eta}. \tag{A2}$$

Here we keep the explicit dependence of μ temporarily for the sake of proving the particle-hole symmetry. In these two equations, $j = x, y$ refer to spatial coordinates, the conduction band and valence band are denoted, respectively, by $\lambda = +$ and $\lambda = -$, η

denotes a positive infinitesimal, and $f(x,\mu)$ is the Fermi distribution function. In addition, $f(x,\mu)$, $\varepsilon_\kappa^\lambda(k_x,k_y)$, and $\mathcal{F}_{\lambda,\lambda'}^{\kappa;jj}(k_x,k_y)$ are given as

$$f(x,\mu)=\frac{1}{1+\exp\left[\beta(x-\mu)\right]}, \tag{A3}$$

$$\varepsilon_\kappa^\lambda(k_x,k_y)=\kappa t v_y k_y+\lambda\mathcal{Z}(k_x,k_y), \tag{A4}$$

$$\mathcal{F}_{\lambda,\lambda'}^{\kappa;xx}(k_x,k_y)=\frac{e^2}{2}v_x^2\left\{1+\lambda\lambda'\frac{v_x^2k_x^2-v_y^2k_y^2}{[\mathcal{Z}(k_x,k_y)]^2}\right\}, \tag{A5}$$

$$\begin{aligned}\mathcal{F}_{\lambda,\lambda'}^{\kappa;yy}(k_x,k_y)=&\frac{e^2}{2}v_y^2\left\{t^2(1+\lambda\lambda')+1+\lambda\lambda'\frac{-v_x^2k_x^2+v_y^2k_y^2}{[\mathcal{Z}(k_x,k_y)]^2}+2(\lambda+\lambda')\frac{\kappa t v_y k_y}{\mathcal{Z}(k_x,k_y)}\right\}\\=&\frac{e^2}{2}v_y^2\left\{2t^2\delta_{\lambda\lambda'}+1-\lambda\lambda'\frac{v_x^2k_x^2-v_y^2k_y^2}{[\mathcal{Z}(k_x,k_y)]^2}+4\lambda\delta_{\lambda\lambda'}\frac{\kappa t v_y k_y}{\mathcal{Z}(k_x,k_y)}\right\},\end{aligned} \tag{A6}$$

where $\beta=1/k_BT$ and $\mathcal{Z}(k_x,k_y)=\sqrt{v_x^2k_x^2+v_y^2k_y^2}$. It can be verified that

$$f(x,\mu)=1-f(-x,-\mu), \tag{A7}$$

$$\varepsilon_\kappa^\lambda(k_x,k_y)=-\varepsilon_{-\kappa}^{-\lambda}(k_x,k_y), \tag{A8}$$

$$\mathcal{F}_{\lambda,\lambda'}^{\kappa;jj}(k_x,k_y)=\mathcal{F}_{-\lambda,-\lambda'}^{-\kappa;jj}(k_x,k_y)=\mathcal{F}_{\lambda',\lambda}^{\kappa;jj}(k_x,k_y). \tag{A9}$$

By utilizing these relations, we have

$$\begin{aligned}\sigma_{jj}(\omega,\mu)=&g_s\frac{i}{\omega}\int_{-\infty}^{+\infty}\frac{dk_x}{2\pi}\int_{-\infty}^{+\infty}\frac{dk_y}{2\pi}\sum_{\kappa=\pm}\sum_{\lambda=\pm}\sum_{\lambda'=\pm}\mathcal{F}_{\lambda,\lambda'}^{\kappa;jj}(k_x,k_y)\frac{f\left[\varepsilon_\kappa^\lambda(k_x,k_y),\mu\right]-f\left[\varepsilon_\kappa^{\lambda'}(k_x,k_y),\mu\right]}{\omega+\varepsilon_\kappa^\lambda(k_x,k_y)-\varepsilon_\kappa^{\lambda'}(k_x,k_y)+i\eta}\\=&g_s\frac{i}{\omega}\int_{-\infty}^{+\infty}\frac{dk_x}{2\pi}\int_{-\infty}^{+\infty}\frac{dk_y}{2\pi}\sum_{\kappa=\pm}\sum_{\lambda=\pm}\sum_{\lambda'=\pm}\mathcal{F}_{\lambda,\lambda'}^{\kappa;jj}(k_x,k_y)\frac{f\left[-\varepsilon_\kappa^{\lambda'}(k_x,k_y),-\mu\right]-f\left[-\varepsilon_\kappa^{\lambda}(k_x,k_y),-\mu\right]}{\omega+\left[-\varepsilon_\kappa^{\lambda'}(k_x,k_y)\right]-\left[-\varepsilon_\kappa^{\lambda}(k_x,k_y)\right]+i\eta}\\=&g_s\frac{i}{\omega}\int_{-\infty}^{+\infty}\frac{dk_x}{2\pi}\int_{-\infty}^{+\infty}\frac{dk_y}{2\pi}\sum_{\kappa=\pm}\sum_{\lambda=\pm}\sum_{\lambda'=\pm}\mathcal{F}_{-\lambda',-\lambda}^{-\kappa;jj}(k_x,k_y)\frac{f\left[-\varepsilon_{-\kappa}^{-\lambda}(k_x,k_y),-\mu\right]-f\left[\varepsilon_{-\kappa}^{-\lambda'}(k_x,k_y),-\mu\right]}{\omega+\left[-\varepsilon_{-\kappa}^{-\lambda}(k_x,k_y)\right]-\left[\varepsilon_{-\kappa}^{-\lambda'}(k_x,k_y)\right]+i\eta}\\=&g_s\frac{i}{\omega}\int_{-\infty}^{+\infty}\frac{dk_x}{2\pi}\int_{-\infty}^{+\infty}\frac{dk_y}{2\pi}\sum_{\kappa=\pm}\sum_{\lambda=\pm}\sum_{\lambda'=\pm}\mathcal{F}_{\lambda',\lambda}^{\kappa;jj}(k_x,k_y)\frac{f\left[\varepsilon_\kappa^{\lambda}(k_x,k_y),-\mu\right]-f\left[\varepsilon_\kappa^{\lambda'}(k_x,k_y),-\mu\right]}{\omega+\varepsilon_\kappa^{\lambda}(k_x,k_y)-\varepsilon_\kappa^{\lambda'}(k_x,k_y)+i\eta}\\=&g_s\frac{i}{\omega}\int_{-\infty}^{+\infty}\frac{dk_x}{2\pi}\int_{-\infty}^{+\infty}\frac{dk_y}{2\pi}\sum_{\kappa=\pm}\sum_{\lambda=\pm}\sum_{\lambda'=\pm}\mathcal{F}_{\lambda,\lambda'}^{\kappa;jj}(k_x,k_y)\frac{f\left[\varepsilon_\kappa^{\lambda}(k_x,k_y),-\mu\right]-f\left[\varepsilon_\kappa^{\lambda'}(k_x,k_y),-\mu\right]}{\omega+\varepsilon_\kappa^{\lambda}(k_x,k_y)-\varepsilon_\kappa^{\lambda'}(k_x,k_y)+i\eta}\\=&\sigma_{jj}(\omega,-\mu),\end{aligned} \tag{A10}$$

which indicates $\sigma_{jj}(\omega,\mu)$ respects the particle-hole symmetry, namely,

$$\sigma_{jj}(\omega,\mu)=\sigma_{jj}(\omega,-\mu)=\sigma_{jj}(\omega,|\mu|). \tag{A11}$$

Keeping this property of $\sigma_{jj}(\omega,\mu)$ in mind, we can safely replace μ in all of $\sigma_{jj}(\omega,\mu)$, $\sigma_{jj}^\kappa(\omega,\mu)$, and $f(x,\mu)$ by $|\mu|$ since we are only concerned with the final result of $\sigma_{jj}(\omega,\mu)$. Hereafter, we restrict our analysis to the n-doped case ($\mu>0$). For simplicity, we further denote $\sigma_{jj}(\omega,\mu)\equiv\sigma_{jj}(\omega)$, $\sigma_{jj}^\kappa(\omega,\mu)\equiv\sigma_{jj}^\kappa(\omega)$, and $f(x,\mu)\equiv f(x)$. Consequently, we have

$$\begin{aligned}\sigma_{jj}(\omega)\equiv\sigma_{jj}(\omega,\mu)=&g_s\frac{i}{\omega}\int_{-\infty}^{+\infty}\frac{dk_x}{2\pi}\int_{-\infty}^{+\infty}\frac{dk_y}{2\pi}\sum_{\kappa=\pm}\sum_{\lambda=\pm}\sum_{\lambda'=\pm}\mathcal{F}_{\lambda,\lambda'}^{\kappa;jj}(k_x,k_y)\frac{f\left[\varepsilon_\kappa^{\lambda}(k_x,k_y),\mu\right]-f\left[\varepsilon_\kappa^{\lambda'}(k_x,k_y),\mu\right]}{\omega+\varepsilon_\kappa^{\lambda}(k_x,k_y)-\varepsilon_\kappa^{\lambda'}(k_x,k_y)+i\eta}\\\equiv&g_s\frac{i}{\omega}\int_{-\infty}^{+\infty}\frac{dk_x}{2\pi}\int_{-\infty}^{+\infty}\frac{dk_y}{2\pi}\sum_{\kappa=\pm}\sum_{\lambda=\pm}\sum_{\lambda'=\pm}\mathcal{F}_{\lambda,\lambda'}^{\kappa;jj}(k_x,k_y)\frac{f\left[\varepsilon_\kappa^{\lambda}(k_x,k_y)\right]-f\left[\varepsilon_\kappa^{\lambda'}(k_x,k_y)\right]}{\omega+\varepsilon_\kappa^{\lambda}(k_x,k_y)-\varepsilon_\kappa^{\lambda'}(k_x,k_y)+i\eta},\end{aligned} \tag{A12}$$

$$\sigma_{jj}^{\kappa}(\omega) \equiv \sigma_{jj}^{\kappa}(\omega,\mu) = \frac{i}{\omega}\int_{-\infty}^{+\infty}\frac{dk_x}{2\pi}\int_{-\infty}^{+\infty}\frac{dk_y}{2\pi}\sum_{\lambda=\pm}\sum_{\lambda'=\pm}\mathcal{F}_{\lambda,\lambda'}^{\kappa;jj}(k_x,k_y)\frac{f\left[\varepsilon_{\kappa}^{\lambda}(k_x,k_y),\mu\right]-f\left[\varepsilon_{\kappa}^{\lambda'}(k_x,k_y),\mu\right]}{\omega+\varepsilon_{\kappa}^{\lambda}(k_x,k_y)-\varepsilon_{\kappa}^{\lambda'}(k_x,k_y)+i\eta}$$
$$\equiv \frac{i}{\omega}\int_{-\infty}^{+\infty}\frac{dk_x}{2\pi}\int_{-\infty}^{+\infty}\frac{dk_y}{2\pi}\sum_{\lambda=\pm}\sum_{\lambda'=\pm}\mathcal{F}_{\lambda,\lambda'}^{\kappa;jj}(k_x,k_y)\frac{f\left[\varepsilon_{\kappa}^{\lambda}(k_x,k_y)\right]-f\left[\varepsilon_{\kappa}^{\lambda'}(k_x,k_y)\right]}{\omega+\varepsilon_{\kappa}^{\lambda}(k_x,k_y)-\varepsilon_{\kappa}^{\lambda'}(k_x,k_y)+i\eta}. \tag{A13}$$

2. Definition and particle-hole symmetry of JDOS

The JDOS for the photon frequency ω and chemical potential μ is given by

$$\mathcal{J}(\omega,\mu) = g_s\sum_{\kappa=\pm}\mathcal{J}_{\kappa}(\omega,\mu), \tag{A14}$$

where

$$\mathcal{J}_{\kappa}(\omega,\mu) = \int\frac{d^2\boldsymbol{k}}{(2\pi)^2}\delta[\varepsilon_{\kappa}^{+}(k_x,k_y)-\varepsilon_{\kappa}^{-}(k_x,k_y)-\omega]\{\Theta[\mu-\varepsilon_{\kappa}^{-}(k_x,k_y)]-\Theta[\mu-\varepsilon_{\kappa}^{+}(k_x,k_y)]\}. \tag{A15}$$

Here we keep the explicit dependence of μ temporarily for the sake of proving the particle-hole symmetry. After introducing $\tilde{k}_x = v_x k_x$ and $\tilde{k}_y = v_y k_y$, the JDOS can be written as

$$\mathcal{J}_{\kappa}(\omega,\mu) = \frac{1}{4\pi^2 v_x v_y}\int d\tilde{k}_x d\tilde{k}_y\delta[\tilde{\varepsilon}_{\kappa}^{+}(\tilde{k}_x,\tilde{k}_y)-\tilde{\varepsilon}_{\kappa}^{-}(\tilde{k}_x,\tilde{k}_y)-\omega]\{\Theta[\mu-\tilde{\varepsilon}_{\kappa}^{-}(\tilde{k}_x,\tilde{k}_y)]-\Theta[\mu-\tilde{\varepsilon}_{\kappa}^{+}(\tilde{k}_x,\tilde{k}_y)]\}$$
$$= \frac{\mathcal{J}_0}{2\pi}\int d\tilde{k}_x d\tilde{k}_y\delta[\tilde{\varepsilon}_{\kappa}^{+}(\tilde{k}_x,\tilde{k}_y)-\tilde{\varepsilon}_{\kappa}^{-}(\tilde{k}_x,\tilde{k}_y)-\omega]\{\Theta[\mu-\tilde{\varepsilon}_{\kappa}^{-}(\tilde{k}_x,\tilde{k}_y)]-\Theta[\mu-\tilde{\varepsilon}_{\kappa}^{+}(\tilde{k}_x,\tilde{k}_y)]\}, \tag{A16}$$

where $\mathcal{J}_0 = 1/(2\pi v_x v_y)$ and $\tilde{\varepsilon}_{\kappa}^{\lambda}(\tilde{k}_x,\tilde{k}_y) = \kappa t\tilde{k}_y + \lambda\sqrt{\tilde{k}_x^2+\tilde{k}_y^2}$.

In the polar coordinate, $\tilde{\varepsilon}_{\kappa}^{\lambda}(\tilde{k}_x,\tilde{k}_y) = [\lambda+\kappa t\sin\phi]\tilde{k}$ and $\tilde{\varepsilon}_{\kappa}^{+}(\tilde{k}_x,\tilde{k}_y)-\tilde{\varepsilon}_{\kappa}^{-}(\tilde{k}_x,\tilde{k}_y) = 2\tilde{k}$. Solving the equation

$$\tilde{\varepsilon}_{\kappa}^{\lambda}(\tilde{k}_x,\tilde{k}_y) = [\lambda+\kappa t\sin\phi]\tilde{k}_F(\kappa,\lambda,\mu) = \mu, \tag{A17}$$

we have the Fermi wave vectors

$$\tilde{k}_F(\kappa,\lambda,\mu) = \frac{\mu}{\lambda+\kappa t\sin\phi} = \frac{\mathrm{sgn}(\mu)|\mu|}{\lambda+\kappa t\sin\phi} = \frac{|\mu|}{\mathrm{sgn}(\mu)\lambda+\mathrm{sgn}(\mu)\kappa t\sin\phi}$$
$$= \tilde{k}_F^{\kappa,\lambda}(\mu)[\Theta(1-t)\delta_{\lambda,\mathrm{sgn}(\mu)}+\Theta(t-1)(\delta_{\lambda,\mathrm{sgn}(\mu)}+\delta_{\lambda,-\mathrm{sgn}(\mu)})] \tag{A18}$$

satisfying the relation

$$\tilde{k}_F^{\kappa,\lambda}(-\mu) = \tilde{k}_F^{-\kappa,-\lambda}(\mu). \tag{A19}$$

From the above two relations, the JDOS can be rewritten as

$$\mathcal{J}(\omega,\mu) = \tilde{\Theta}(t)[\tilde{\Theta}(1-t)+\Theta(t-1)]\mathcal{J}(\omega,\mu) = \tilde{\Theta}(t)[\tilde{\Theta}(1-t)+\Theta(t-1)]\sum_{\kappa=\pm}\mathcal{J}_{\kappa}(\omega,\mu)$$
$$= \tilde{\Theta}(t)[\tilde{\Theta}(1-t)+\Theta(t-1)]\sum_{\kappa=\pm}\frac{\mathcal{J}_0}{2\pi}\int d\tilde{k}_x d\tilde{k}_y\delta[2\tilde{k}-\omega]\{\Theta[\mu-\tilde{\varepsilon}_{\kappa}^{-}(\tilde{k}_x,\tilde{k}_y)]-\Theta[\mu-\tilde{\varepsilon}_{\kappa}^{+}(\tilde{k}_x,\tilde{k}_y)]\}$$
$$= \tilde{\Theta}(t)\tilde{\Theta}(1-t)\frac{\mathcal{J}_0}{2\pi}\int_{-\infty}^{\infty}\int_{-\infty}^{\infty}d\tilde{k}_x d\tilde{k}_y\delta[2\tilde{k}-\omega]\sum_{\kappa=\pm}\sum_{\lambda=\pm}\Theta[\omega-2\tilde{k}_F(\kappa,\lambda,\mu)]$$
$$+\ \tilde{\Theta}(t)\Theta(t-1)\frac{\mathcal{J}_0}{2\pi}\int_{-\infty}^{\infty}\int_{-\infty}^{\infty}d\tilde{k}_x d\tilde{k}_y\delta[2\tilde{k}-\omega]\sum_{\kappa=\pm}\sum_{\lambda=\pm}\Theta\{\mathrm{sgn}(\mu)[\tilde{k}_F^{\kappa,-}(\mu)-\tilde{k}_F^{\kappa,+}(\mu)]\}\Theta[\omega-2\tilde{k}_F(\kappa,\lambda,\mu)]$$
$$= \tilde{\Theta}(t)\tilde{\Theta}(1-t)\frac{\mathcal{J}_0}{2\pi}\int_{-\infty}^{\infty}\int_{-\infty}^{\infty}d\tilde{k}_x d\tilde{k}_y\delta[2\tilde{k}-\omega]\sum_{\kappa=\pm}\sum_{\lambda=\pm}\Theta[\omega-2\tilde{k}_F^{\kappa,\lambda}(\mu)\delta_{\lambda,\mathrm{sgn}(\mu)}]$$
$$+\ \tilde{\Theta}(t)\Theta(t-1)\frac{\mathcal{J}_0}{2\pi}\int_{-\infty}^{\infty}\int_{-\infty}^{\infty}d\tilde{k}_x d\tilde{k}_y\delta[2\tilde{k}-\omega]\sum_{\kappa=\pm}\sum_{\lambda=\pm}\Theta\{\mathrm{sgn}(\mu)[\tilde{k}_F^{\kappa,-}(\mu)-\tilde{k}_F^{\kappa,+}(\mu)]\}$$
$$\times\ \{\Theta[\omega-2\tilde{k}_F^{\kappa,\lambda}(\mu)\delta_{\lambda,\mathrm{sgn}(\mu)}]-\Theta[\omega-2\tilde{k}_F^{\kappa,\lambda}(\mu)\delta_{\lambda,\mathrm{sgn}(-\mu)}]\}. \tag{A20}$$

Consequently, we have

$$\begin{aligned}
\mathcal{J}(\omega,-\mu) &= \tilde{\Theta}(t)\tilde{\Theta}(1-t)\frac{\mathcal{J}_0}{2\pi}\int_{-\infty}^{\infty}\int_{-\infty}^{\infty}d\tilde{k}_x d\tilde{k}_y \delta[2\tilde{k}-\omega]\sum_{\kappa=\pm}\sum_{\lambda=\pm}\Theta[\omega-2\tilde{k}_F^{\kappa,\lambda}(-\mu)\delta_{\lambda,\mathrm{sgn}(-\mu)}] \\
&+ \tilde{\Theta}(t)\Theta(t-1)\frac{\mathcal{J}_0}{2\pi}\int_{-\infty}^{\infty}\int_{-\infty}^{\infty}d\tilde{k}_x d\tilde{k}_y \delta[2\tilde{k}-\omega]\sum_{\kappa=\pm}\sum_{\lambda=\pm}\Theta\{\mathrm{sgn}(-\mu)[\tilde{k}_F^{\kappa,-}(-\mu)-\tilde{k}_F^{\kappa,+}(-\mu)]\} \\
&\times \left\{\Theta\left[\omega-2\tilde{k}_F^{\kappa,\lambda}(-\mu)\delta_{\lambda,\mathrm{sgn}(-\mu)}\right]-\Theta\left[\omega-2\tilde{k}_F^{\kappa,\lambda}(-\mu)\delta_{\lambda,-\mathrm{sgn}(-\mu)}\right]\right\} \\
&= \tilde{\Theta}(t)\tilde{\Theta}(1-t)\frac{\mathcal{J}_0}{2\pi}\int_{-\infty}^{\infty}\int_{-\infty}^{\infty}d\tilde{k}_x d\tilde{k}_y \delta[2\tilde{k}-\omega]\sum_{\kappa=\pm}\sum_{\lambda=\pm}\Theta\left[\omega-2\tilde{k}_F^{-\kappa,-\lambda}(\mu)\delta_{-\lambda,\mathrm{sgn}(\mu)}\right] \\
&+ \tilde{\Theta}(t)\Theta(t-1)\frac{\mathcal{J}_0}{2\pi}\int_{-\infty}^{\infty}\int_{-\infty}^{\infty}d\tilde{k}_x d\tilde{k}_y \delta[2\tilde{k}-\omega]\sum_{\kappa=\pm}\sum_{\lambda=\pm}\Theta\left\{-\mathrm{sgn}(\mu)\left[\tilde{k}_F^{-\kappa,+}(\mu)-\tilde{k}_F^{-\kappa,-}(\mu)\right]\right\} \\
&\times \left\{\Theta\left[\omega-2\tilde{k}_F^{-\kappa,-\lambda}(\mu)\delta_{-\lambda,\mathrm{sgn}(\mu)}\right]-\Theta\left[\omega-2\tilde{k}_F^{-\kappa,-\lambda}(\mu)\delta_{-\lambda,\mathrm{sgn}(-\mu)}\right]\right\} \\
&= \tilde{\Theta}(t)\tilde{\Theta}(1-t)\frac{\mathcal{J}_0}{2\pi}\int_{-\infty}^{\infty}\int_{-\infty}^{\infty}d\tilde{k}_x d\tilde{k}_y \delta[2\tilde{k}-\omega]\sum_{\kappa=\pm}\sum_{\lambda=\pm}\Theta\left[\omega-2\tilde{k}_F^{\kappa,\lambda}(\mu)\delta_{\lambda,\mathrm{sgn}(\mu)}\right] \\
&+ \tilde{\Theta}(t)\Theta(t-1)\frac{\mathcal{J}_0}{2\pi}\int_{-\infty}^{\infty}\int_{-\infty}^{\infty}d\tilde{k}_x d\tilde{k}_y \delta[2\tilde{k}-\omega]\sum_{\kappa=\pm}\sum_{\lambda=\pm}\Theta\left\{\mathrm{sgn}(\mu)\left[\tilde{k}_F^{\kappa,-}(\mu)-\tilde{k}_F^{\kappa,+}(\mu)\right]\right\} \\
&\times \left\{\Theta\left[\omega-2\tilde{k}_F^{\kappa,\lambda}(\mu)\delta_{\lambda,\mathrm{sgn}(\mu)}\right]-\Theta\left[\omega-2\tilde{k}_F^{\kappa,\lambda}(\mu)\delta_{\lambda,\mathrm{sgn}(-\mu)}\right]\right\} \\
&= \mathcal{J}(\omega,\mu). \qquad \text{(A21)}
\end{aligned}$$

Obviously, $\mathcal{J}(\omega,\mu)$ respects the particle-hole symmetry, namely,

$$\mathcal{J}(\omega,\mu)=\mathcal{J}(\omega,-\mu)=\mathcal{J}(\omega,|\mu|). \qquad \text{(A22)}$$

Keeping this property of $\mathcal{J}(\omega,\mu)$ in mind, we can safely replace μ in all of $\mathcal{J}(\omega,\mu)$, $\mathcal{J}_\kappa(\omega,\mu)$, and $\Theta(x,\mu)$ by $|\mu|$ since we are only concerned with the final result of $\mathcal{J}(\omega,\mu)$. Hereafter, we are allowed to restrict our analysis to the n-doped case ($\mu>0$). For simplicity, we further denote $\mathcal{J}(\omega,\mu)\equiv\mathcal{J}(\omega)$, $\mathcal{J}_\kappa(\omega,\mu)\equiv\mathcal{J}_\kappa(\omega)$, and $\Theta(x,\mu)\equiv\Theta(x)$.

APPENDIX B: DETAILED CALCULATION OF LOC

In the following, we present the detailed calculation of them in the n-doped case ($\mu>0$). Before doing that, we factor the ratio v_y/v_x or v_x/v_y out from the original expressions in order to simplify the calculation. This way, the original expressions in the *anisotropic model* ($v_x\neq v_y$ and $v_t\geqslant 0$) are converted to be the rescaled forms in the *isotropic model* ($v_x=v_y$ and $v_t\geqslant 0$). Next we focus on the interband part and intraband part of LOC, respectively.

1. Calculation of interband LOC

After substituting $\tilde{k}_x=v_x k_x$ and $\tilde{k}_y=v_y k_y$ into Eq. (10) and expressing it in terms of $\tilde{k}=\sqrt{\tilde{k}_x^2+\tilde{k}_y^2}$ and $\phi=\arctan(\tilde{k}_y/\tilde{k}_x)$, the original expressions in the anisotropic model are converted to be the rescaled forms in the isotropic model as

$$\mathrm{Re}\sigma^{\kappa}_{jj(\mathrm{IB})}(\omega)=\int\frac{d\tilde{k}_x d\tilde{k}_y}{4\pi v_x v_y}\tilde{\mathcal{F}}^{\kappa;jj}_{-,+}(\tilde{k}_x,\tilde{k}_y)\frac{f[\kappa t\tilde{k}_y-\tilde{k}]-f[\kappa t\tilde{k}_y+\tilde{k}]}{\omega}\delta[\omega-2\tilde{k}], \qquad \text{(B1)}$$

where

$$\begin{aligned}
\tilde{\mathcal{F}}^{\kappa;xx}_{-,+}(\tilde{k}_x,\tilde{k}_y) &= 4\sigma_0\frac{v_x^2\tilde{k}_y^2}{\tilde{k}^2}=4\sigma_0 v_x^2\sin^2\phi, \\
\tilde{\mathcal{F}}^{\kappa;yy}_{-,+}(\tilde{k}_x,\tilde{k}_y) &= 4\sigma_0\frac{v_y^2\tilde{k}_x^2}{\tilde{k}^2}=4\sigma_0 v_y^2\cos^2\phi.
\end{aligned}$$

As a consequence, the ratio v_y/v_x or v_x/v_y can be factored out from the original expressions as

$$\mathrm{Re}\sigma^{\kappa}_{xx(\mathrm{IB})}(\omega)=\sigma_0\frac{v_x}{v_y}\Gamma^{\kappa}_{xx(\mathrm{IB})}(\omega), \qquad \text{(B2)}$$

$$\mathrm{Re}\sigma^{\kappa}_{yy(\mathrm{IB})}(\omega)=\sigma_0\frac{v_y}{v_x}\Gamma^{\kappa}_{yy(\mathrm{IB})}(\omega), \qquad \text{(B3)}$$

where two dimensionless auxiliary functions

$$\Gamma^{\kappa}_{xx(\mathrm{IB})}(\omega)=\int_0^{+\infty}\frac{\tilde{k}d\tilde{k}}{\omega}\int_0^{2\pi}\frac{\sin^2\phi\,d\phi}{\pi}\delta[\omega-2\tilde{k}]\{f[(\kappa t\sin\phi-1)\tilde{k}]-f[(\kappa t\sin\phi+1)\tilde{k}]\}$$
$$=\int_0^{+\infty}\frac{\tilde{k}d\tilde{k}}{\omega}\int_{-\pi/2}^{3\pi/2}\frac{\sin^2\phi\,d\phi}{\pi}\delta[\omega-2\tilde{k}]\{f[(\kappa t\sin\phi-1)\tilde{k}]-f[(\kappa t\sin\phi+1)\tilde{k}]\},\tag{B4}$$

$$\Gamma^{\kappa}_{yy(\mathrm{IB})}(\omega)=\int_0^{+\infty}\frac{\tilde{k}\,d\tilde{k}}{\omega}\int_{-\pi/2}^{3\pi/2}\frac{\cos^2\phi\,d\phi}{\pi}\delta[\omega-2\tilde{k}]\{f[(\kappa t\sin\phi-1)\tilde{k}]-f[(\kappa t\sin\phi+1)\tilde{k}]\}\tag{B5}$$

are introduced for convenience. The ratio v_x/v_y in $\mathrm{Re}\sigma^{\kappa}_{xx(\mathrm{IB})}(\omega)$ and v_y/v_x in $\mathrm{Re}\sigma^{\kappa}_{yy(\mathrm{IB})}(\omega)$ are totally different in the anisotropic model but the same in the isotropic model. Therefore, the calculation of $\mathrm{Re}\sigma^{\kappa}_{xx(\mathrm{IB})}(\omega)$ and $\mathrm{Re}\sigma^{\kappa}_{yy(\mathrm{IB})}(\omega)$ boils down to calculating $\Gamma^{\kappa}_{xx(\mathrm{IB})}(\omega)$ and $\Gamma^{\kappa}_{yy(\mathrm{IB})}(\omega)$. Integrating over $\tilde{k}$ leads us to

$$\Gamma^{\kappa}_{xx(\mathrm{IB})}(\omega)=\frac{1}{4}\int_{-\pi/2}^{3\pi/2}\frac{\sin^2\phi\,d\phi}{\pi}\left\{f\left[(\kappa t\sin\phi-1)\frac{\omega}{2}\right]-f\left[(\kappa t\sin\phi+1)\frac{\omega}{2}\right]\right\}$$
$$=\frac{1}{4}\int_{-\pi/2}^{\pi/2}\frac{\sin^2\phi\,d\phi}{\pi}\left\{f\left[(\kappa t\sin\phi-1)\frac{\omega}{2}\right]-f\left[(\kappa t\sin\phi+1)\frac{\omega}{2}\right]+f\left[(-\kappa t\sin\phi-1)\frac{\omega}{2}\right]-f\left[(-\kappa t\sin\phi+1)\frac{\omega}{2}\right]\right\},$$

and hence

$$\Gamma^{\mathrm{IB}}_{xx}(\omega)=g_s[\Gamma^{+}_{xx(\mathrm{IB})}(\omega)+\Gamma^{-}_{xx(\mathrm{IB})}(\omega)]$$
$$=\int_{-\pi/2}^{\pi/2}\frac{\sin^2\phi\,d\phi}{\pi}\left\{f\left[(t\sin\phi-1)\frac{\omega}{2}\right]-f\left[(t\sin\phi+1)\frac{\omega}{2}\right]+f\left[(-t\sin\phi-1)\frac{\omega}{2}\right]-f\left[(-t\sin\phi+1)\frac{\omega}{2}\right]\right\},$$

which includes the contribution of different valleys, where $g_s=2$ is the degeneracy parameter of spin. Parallel procedures give rise to

$$\Gamma^{\mathrm{IB}}_{yy}(\omega)=g_s[\Gamma^{+}_{yy(\mathrm{IB})}(\omega)+\Gamma^{-}_{yy(\mathrm{IB})}(\omega)]$$
$$=\int_{-\pi/2}^{\pi/2}\frac{\cos^2\phi\,d\phi}{\pi}\left\{f\left[(t\sin\phi-1)\frac{\omega}{2}\right]-f\left[(t\sin\phi+1)\frac{\omega}{2}\right]+f\left[(-t\sin\phi-1)\frac{\omega}{2}\right]-f\left[(-t\sin\phi+1)\frac{\omega}{2}\right]\right\}.\tag{B6}$$

In order to obtain the analytical expressions, we perform the integrations over ϕ at zero temperature where the Fermi distribution function $f(x)$ can be replaced by the Heaviside step function $\Theta[\mu-x]$ and consequently have

$$\Gamma^{\mathrm{IB}}_{xx}(\omega)=\int_{-\pi/2}^{\pi/2}\frac{2\sin^2\phi\,d\phi}{\pi}\left\{\Theta\left[\mu-(t\sin\phi-1)\frac{\omega}{2}\right]-\Theta\left[\mu-(t\sin\phi+1)\frac{\omega}{2}\right]\right\}$$
$$=\int_{-1}^{1}\frac{2x^2dx}{\pi\sqrt{1-x^2}}\left\{\Theta\left[\mu-(tx-1)\frac{\omega}{2}\right]-\Theta\left[\mu-(tx+1)\frac{\omega}{2}\right]\right\}\tag{B7}$$

and

$$\Gamma^{\mathrm{IB}}_{yy}(\omega)=\int_{-\pi/2}^{\pi/2}\frac{2\cos^2\phi\,d\phi}{\pi}\left\{\Theta\left[\mu-(t\sin\phi-1)\frac{\omega}{2}\right]-\Theta\left[\mu-(t\sin\phi+1)\frac{\omega}{2}\right]\right\}$$
$$=\int_{-1}^{1}\frac{2\sqrt{1-x^2}dx}{\pi}\left\{\Theta\left[\mu-(tx-1)\frac{\omega}{2}\right]-\Theta\left[\mu-(tx+1)\frac{\omega}{2}\right]\right\}.\tag{B8}$$

After rewriting the Heaviside step function, we get

$$\Gamma^{\mathrm{IB}}_{xx}(\omega)=\int_{-1}^{1}\frac{2x^2dx}{\pi\sqrt{1-x^2}}\left\{\Theta\left[-x+\frac{2\mu/\omega+1}{t}\right]-\Theta\left[-x+\frac{2\mu/\omega-1}{t}\right]\right\}$$
$$=\int_{-1}^{1}\frac{2x^2dx}{\pi\sqrt{1-x^2}}\{\Theta[-x+\xi_+]-\Theta[-x+\xi_-]\}\tag{B9}$$

and

$$\Gamma^{\mathrm{IB}}_{yy}(\omega)=\int_{-1}^{1}\frac{2\sqrt{1-x^2}dx}{\pi}\{\Theta[-x+\xi_+]-\Theta[-x+\xi_-]\},\tag{B10}$$

with $\xi_{\pm}=\frac{2\mu\pm\omega}{\omega}\frac{\Theta(t)}{t}$.

By imposing constraints on the integration interval via the Heaviside step function, $\Gamma^{\mathrm{IB}}_{jj}(\omega)$ can be obtained for the type-I, type-II, and type-III Dirac bands as follows.

a. Interband LOC for type-I phase

For the type-I phase ($0 < t < 1$), due to $\xi_+ = (2\mu/\omega + 1)\frac{\Theta(t)}{t} > 1$, we have $\Theta[-x+\xi_+] = 1$. The energy ω have three regions determined by the Heaviside step function $\Theta[-x+\xi_-]$, which are $0 < \omega < \frac{2\mu}{t+1}$ for $\Theta[-x+\xi_-] = 1$ at $-1 < x < 1$, $\frac{2\mu}{t+1} \leqslant \omega < \frac{2\mu}{t-1}$ for $\Theta[-x+\xi_-] = 1$ at $-1 < x < \xi_-$, and $\omega \geqslant \frac{2\mu}{t-1}$ for $\Theta[-x+\xi_-] = 0$ at $-1 < x < 1$. The $\Gamma^{\mathrm{IB}}_{jj}(\omega)$ are given by

$$\Gamma^{\mathrm{IB}}_{xx}(\omega) = 1 - \int_{-1}^{1} \frac{2x^2 dx}{\pi\sqrt{1-x^2}}\Theta[-x+\xi_-] = \begin{cases} 0, & 0 < \omega < \omega_1(t) \\ 1 - G_-(\xi_-), & \omega_1(t) \leqslant \omega < \omega_2(t) \\ 1, & \omega \geqslant \omega_2(t) \end{cases} \tag{B11}$$

and

$$\Gamma^{\mathrm{IB}}_{yy}(\omega) = 1 - \int_{-1}^{1} \frac{2\sqrt{1-x^2} dx}{\pi}\Theta[-x+\xi_-] = \begin{cases} 0, & 0 < \omega < \omega_1(t) \\ 1 - G_+(\xi_-), & \omega_1(t) \leqslant \omega < \omega_2(t) \\ 1, & \omega \geqslant \omega_2(t), \end{cases} \tag{B12}$$

where

$$\begin{aligned} \omega_1(t) =& 2\mu\frac{\Theta(t)}{1+t}, \\ \omega_2(t) =& 2\mu\Theta(t)\left[\frac{\Theta(1-t)}{1-t} + \frac{\Theta(t-1)}{t-1}\right], \\ G_\pm(x) =& \frac{1}{2} + \frac{\arcsin x}{\pi} \pm \frac{x\sqrt{1-x^2}}{\pi}. \end{aligned} \tag{B13}$$

b. Interband LOC for type-II phase

At the type-II phase ($t > 1$), the Heaviside step function $\Theta[-x+\xi_+]$ is equal to 1, when $0 < \omega < \frac{2\mu}{t-1}$ for $x \in (-1, 1)$, and when $\omega \geqslant \frac{2\mu}{t-1}$ for $x \in (-1, \xi_+)$. The second Heaviside step function satisfies $\Theta[-x+\xi_-] = 1$ when $0 < \omega < \frac{2\mu}{t+1}$ for $x \in (-1, 1)$, and when $\omega \geqslant \frac{2\mu}{t+1}$ for $x \in (-1, \xi_-)$ so that there are three regions of the energy ω, which are $0 < \omega < \frac{2\mu}{t+1}$, $\frac{2\mu}{t+1} \leqslant \omega < \frac{2\mu}{t-1}$, and $\omega \geqslant \frac{2\mu}{t-1}$. So, we have

$$\Gamma^{\mathrm{IB}}_{xx}(\omega) = \int_{-1}^{1} \frac{2x^2 dx}{\pi\sqrt{1-x^2}}\{\Theta[-x+\xi_+] - \Theta[-x+\xi_-]\} = \begin{cases} 0, & 0 < \omega < \omega_1(t) \\ 1 - G_-(\xi_-), & \omega_1(t) \leqslant \omega < \omega_2(t) \\ \sum_{\chi=\pm1} \chi G_-(\xi_\chi), & \omega \geqslant \omega_2(t) \end{cases} \tag{B14}$$

and

$$\Gamma^{\mathrm{IB}}_{yy}(\omega) = \int_{-1}^{1} \frac{2\sqrt{1-x^2} dx}{\pi}\{\Theta[-x+\xi_+] - \Theta[-x+\xi_-]\} = \begin{cases} 0, & 0 < \omega < \omega_1(t) \\ 1 - G_+(\xi_-), & \omega_1(t) \leqslant \omega < \omega_2(t) \\ \sum_{\chi=\pm1} \chi G_+(\xi_\chi), & \omega \geqslant \omega_2(t). \end{cases} \tag{B15}$$

c. Interband LOC for type-III phase

For the type-III phase ($t = 1$), due to $\xi_+ = 2\mu/\omega + 1 > 1$, we have $\Theta[-x+\xi_+] = 1$, and now the ξ_- is $\xi_- = 2\mu/\omega - 1$. The energy ω has two regions by solving the Heaviside step function $\Theta[-x+\xi_-] = 1$ or 0, which are $0 < \omega < \mu$ and $\omega \geqslant \mu$. The $\Gamma^{\mathrm{IB}}_{jj}(\omega)$ are given by

$$\Gamma^{\mathrm{IB}}_{xx}(\omega) = 1 - \int_{-1}^{1} \frac{2x^2 dx}{\pi\sqrt{1-x^2}}\Theta[-x+\xi_-] = \begin{cases} 0, & 0 < \omega < \mu \\ 1 - G_-(\xi_-), & \omega \geqslant \mu \end{cases} \tag{B16}$$

and

$$\Gamma^{\mathrm{IB}}_{yy}(\omega) = 1 - \int_{-1}^{1} \frac{2\sqrt{1-x^2} dx}{\pi}\Theta[-x+\xi_-] = \begin{cases} 0, & 0 < \omega < \mu \\ 1 - G_+(\xi_-), & \omega \geqslant \mu. \end{cases} \tag{B17}$$

2. Detailed calculation of intraband LOC

After substituting $\tilde{k}_x = v_x k_x$ and $\tilde{k}_y = v_y k_y$ into Eq. (11) and expressing it in terms of $\tilde{k} = \sqrt{\tilde{k}_x^2 + \tilde{k}_y^2}$ and $\phi = \arctan(\tilde{k}_y/\tilde{k}_x)$, the original expressions in the anisotropic model are converted to be the rescaled forms in the isotropic model as

$$\mathrm{Re}\sigma^{\kappa,\lambda}_{jj(\mathrm{D})}(\omega) = \int \frac{d\tilde{k}_x d\tilde{k}_y}{4\pi v_x v_y} \tilde{\mathcal{F}}^{\kappa;jj}_{\lambda,\lambda}(\tilde{k}_x, \tilde{k}_y)\left[-\frac{df[\tilde{\varepsilon}^\lambda_\kappa(\tilde{k}_x, \tilde{k}_y)]}{d\tilde{\varepsilon}^\lambda_\kappa(\tilde{k}_x, \tilde{k}_y)}\right]\delta(\omega), \tag{B18}$$

with

$$\tilde{\mathcal{F}}^{\kappa;xx}_{\lambda,\lambda}(\tilde{k}_x,\tilde{k}_y)=4\sigma_0\frac{v_x^2\tilde{k}_x^2}{\tilde{k}^2}=4\sigma_0 v_x^2\cos^2\phi,$$

$$\tilde{\mathcal{F}}^{\kappa;yy}_{\lambda,\lambda}(\tilde{k}_x,\tilde{k}_y)=4\sigma_0 v_y^2\left(t^2+\frac{\tilde{k}_y^2}{\tilde{k}^2}+2\frac{\lambda\kappa t\tilde{k}_y}{\tilde{k}}\right)=4\sigma_0 v_y^2(\sin\phi+\lambda\kappa t)^2,$$

where $\tilde{\varepsilon}^{\lambda}_{\kappa}(\tilde{k}_x,\tilde{k}_y)=\kappa t\tilde{k}_y+\lambda\tilde{k}$.

At zero temperature, the Fermi distribution function $f(x)$ can be replaced by the Heaviside step function $\Theta[\mu-x]$, then the derivative reduces to $\delta[\mu-\tilde{\varepsilon}^{\lambda}_{\kappa}(\tilde{k}_x,\tilde{k}_y)]$. In the polar coordinate, we obtain

$$\begin{aligned}\mathrm{Re}\sigma^{\kappa,\lambda}_{xx(\mathrm{D})}(\omega)&=\frac{\sigma_0}{\pi}\frac{v_x}{v_y}\int_0^{+\infty}\tilde{k}\,d\tilde{k}\int_{-\pi/2}^{3\pi/2}\cos^2\phi\,d\phi\,\delta[\mu-(\kappa t\sin\phi+\lambda)\tilde{k}]\delta(\omega)\\&=\frac{\sigma_0}{\pi}\frac{v_x}{v_y}\int_0^{+\infty}\tilde{k}\,d\tilde{k}\int_{-\pi/2}^{\pi/2}\cos^2\phi\,d\phi\{\delta[\mu-(\kappa t\sin\phi+\lambda)\tilde{k}]+\delta[\mu-(-\kappa t\sin\phi+\lambda)\tilde{k}]\}\delta(\omega),\end{aligned}\tag{B19}$$

$$\begin{aligned}\mathrm{Re}\sigma^{\kappa,\lambda}_{yy(\mathrm{D})}(\omega)&=\frac{\sigma_0}{\pi}\frac{v_y}{v_x}\int_0^{+\infty}\tilde{k}\,d\tilde{k}\int_{-\pi/2}^{3\pi/2}(\sin\phi+\lambda\kappa t)^2d\phi\delta[\mu-(\kappa t\sin\phi+\lambda)\tilde{k}]\delta(\omega)\\&=\frac{\sigma_0}{\pi}\frac{v_y}{v_x}\int_0^{+\infty}\tilde{k}\,d\tilde{k}\int_{-\pi/2}^{\pi/2}(\sin\phi+\lambda\kappa t)^2d\phi\{\delta[\mu-(\kappa t\sin\phi+\lambda)\tilde{k}]+\delta[\mu-(-\kappa t\sin\phi+\lambda)\tilde{k}]\}\delta(\omega).\end{aligned}\tag{B20}$$

As a consequence, the ratio v_y/v_x or v_x/v_y can be factored out from the original expressions as

$$\mathrm{Re}\sigma^{\lambda}_{xx(\mathrm{D})}(\omega)=g_s\big[\mathrm{Re}\sigma^{+,\lambda}_{xx(\mathrm{D})}(\omega)+\mathrm{Re}\sigma^{-,\lambda}_{xx(\mathrm{D})}(\omega)\big]=\sigma_0\frac{v_x}{v_y}\Gamma^{\mathrm{D},\lambda}_{xx}(\mu,t,\Lambda)\delta(\omega),\tag{B21}$$

$$\mathrm{Re}\sigma^{\lambda}_{yy(\mathrm{D})}(\omega)=g_s\big[\mathrm{Re}\sigma^{+,\lambda}_{yy(\mathrm{D})}(\omega)+\mathrm{Re}\sigma^{-,\lambda}_{yy(\mathrm{D})}(\omega)\big]=\sigma_0\frac{v_y}{v_x}\Gamma^{\mathrm{D},\lambda}_{yy}(\mu,t,\Lambda)\delta(\omega),\tag{B22}$$

where two dimensionless auxiliary functions

$$\Gamma^{\mathrm{D},\lambda}_{xx}(\mu,t,\Lambda)=\frac{8}{\pi}\int_0^{+\infty}\tilde{k}\,d\tilde{k}\int_{-\pi/2}^{\pi/2}\cos^2\phi\,d\phi\;\delta\big[\mu-(t\sin\phi+\lambda)\tilde{k}\big],\tag{B23}$$

$$\Gamma^{\mathrm{D},\lambda}_{yy}(\mu,t,\Lambda)=\frac{8}{\pi}\int_0^{+\infty}\tilde{k}\,d\tilde{k}\int_{-\pi/2}^{\pi/2}(\sin\phi+\lambda t)^2d\phi\;\delta\big[\mu-(t\sin\phi+\lambda)\tilde{k}\big]\tag{B24}$$

are introduced for convenience. The ratio v_x/v_y in $\mathrm{Re}\sigma^{\lambda}_{xx(\mathrm{D})}(\omega)$ and v_y/v_x in $\mathrm{Re}\sigma^{\lambda}_{yy(\mathrm{D})}(\omega)$ are totally different in the anisotropic model but the same in the isotropic model. Therefore, the calculation of $\mathrm{Re}\sigma^{\lambda}_{xx(\mathrm{D})}(\omega)$ and v_y/v_x in $\mathrm{Re}\sigma^{\lambda}_{yy(\mathrm{D})}(\omega)$ boils down to calculating $\Gamma^{\mathrm{D},\lambda}_{xx}(\mu,t,\Lambda)$ and $\Gamma^{\mathrm{D},\lambda}_{yy}(\mu,t,\Lambda)$.

a. Intraband LOC for type-I phase

For the type-I phase ($0<t<1$), by replacing $\sin\phi$ with x and integrating over $\tilde{k}$, we get

$$\Gamma^{\mathrm{D},\mathrm{sgn}(\mu)}_{xx}(\mu,t,\Lambda)=\frac{8\mu}{\pi}\int_{-1}^{1}dx\frac{\sqrt{1-x^2}}{[1+\mathrm{sgn}(\mu)tx]^2}=8\mu\frac{1-\sqrt{1-t^2}}{t^2\sqrt{1-t^2}},\tag{B25}$$

$$\Gamma^{\mathrm{D},\mathrm{sgn}(\mu)}_{yy}(\mu,t,\Lambda)=\frac{8\mu}{\pi}\int_{-1}^{1}\frac{dx}{[1+\mathrm{sgn}(\mu)tx]^2}\frac{[x+\mathrm{sgn}(\mu)t]^2}{\sqrt{1-x^2}}=8\mu\frac{1-\sqrt{1-t^2}}{t^2}.\tag{B26}$$

Utilizing the relations

$$\mathrm{Re}\sigma^{\lambda}_{xx(\mathrm{D})}(\omega)=\sigma_0\frac{v_x}{v_y}\Gamma^{\mathrm{D},\mathrm{sgn}(\mu)}_{xx}(\mu,t,\Lambda)\delta(\omega)\equiv\sigma_0\frac{4\mu}{\pi}N_1\delta(\omega),\tag{B27}$$

$$\mathrm{Re}\sigma^{\lambda}_{yy(\mathrm{D})}(\omega)=\sigma_0\frac{v_y}{v_x}\Gamma^{\mathrm{D},\mathrm{sgn}(\mu)}_{yy}(\mu,t,\Lambda)\delta(\omega)\equiv\sigma_0\frac{4\mu}{\pi}N_2\delta(\omega),\tag{B28}$$

we have

$$N_1=2\pi\frac{v_x}{v_y}\frac{1-\sqrt{1-t^2}}{t^2\sqrt{1-t^2}},\tag{B29}$$

$$N_2=2\pi\frac{v_y}{v_x}\frac{1-\sqrt{1-t^2}}{t^2}.\tag{B30}$$

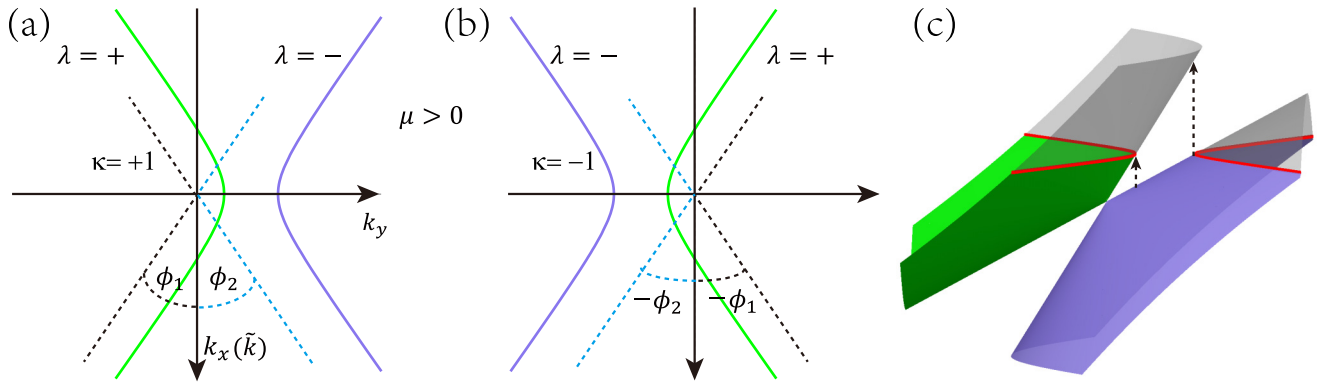

FIG. 5. Schematic diagram of the limitation of the angle ϕ imposed by the delta function in the n-doped case ($\mu > 0$). In the $\kappa = +1$ valley shown in (a), the angle ranges from ϕ_1 to $\pi + |\phi_1|$ for $\lambda = +$, but becomes $(\phi_2, \pi - \phi_2)$ for $\lambda = -$. The case for $\kappa = -$ is shown in (b) for reference. The corresponding optical transitions at the $\kappa = +$ valley are referred to in (c).

These expressions of Drude conductivity yield the numerical results of Drude weight in the Ref. [27], namely, $N_1 = 4.686$ and $N_2 = 2.673$ after substituting the parameters of 8-*Pmmn* borophene ($v_x = 0.86v_F$, $v_y = 0.69v_F$, and $v_t = 0.32v_F$ with $v_F = 10^6 m/s$).

In the limit $t \to 0$, we recover the result for ordinary Dirac cone,

$$\Gamma_{xx}^{\mathrm{D},\mathrm{sgn}(\mu)}(\mu, t = 0, \Lambda) = \Gamma_{yy}^{\mathrm{D},\mathrm{sgn}(\mu)}(\mu, t = 0, \Lambda) = 4\mu = 4\mu\ \mathrm{sgn}(\mu). \tag{B31}$$

In the limit $t \to 1^-$, we have

$$\Gamma_{xx}^{\mathrm{D},\mathrm{sgn}(\mu)}(\mu, t = 1^-, \Lambda) \to \infty, \tag{B32}$$

$$\Gamma_{yy}^{\mathrm{D},\mathrm{sgn}(\mu)}(\mu, t = 1^-, \Lambda) = 8\mu = 8\mu\ \mathrm{sgn}(\mu). \tag{B33}$$

b. Intraband LOC for type-II phase

For the type-II phase ($t > 1$), there is not only an electron pocket but also a hole pocket at one valley. We take $\kappa = +1$ and $\mu > 0$ as an example. In the polar coordinates, there are constraints on the values of $\tilde{k}$ and ϕ. For $\lambda = +1$, $\tilde{k}_{\min} = \mu/(t+1)$, $\phi \in (\phi_1, \pi + |\phi_1|)$ where ϕ_1 is determined by $(t \sin\phi_1 + 1)\Lambda = \mu$, where Λ is the cutoff of $\tilde{k}$. The cut-off Λ is a measure of the density of states due to electron and hole Fermi pockets [79]. For $\lambda = -1$, $\tilde{k}_{\min} = \mu/(t-1)$, $\phi \in (\phi_2, \pi - \phi_2)$, where ϕ_2 is obtained by solving $(t \sin\phi_2 - 1)\Lambda = \mu$. The schematic diagrams of these constraints in the polar coordinate are explicitly shown in Fig. 5.

Consequently, for $\lambda = +1$, $\Gamma_{xx}^{\mathrm{D},+}(\mu, t, \Lambda)$ is given by

$$\begin{aligned}\Gamma_{xx}^{\mathrm{D},+}(\mu, t, \Lambda) &= \frac{8}{\pi}\int_{\mu/(1+t)}^{\Lambda} \tilde{k}\, d\tilde{k} \int_{\phi_1}^{\pi/2} \cos^2\phi\, d\phi\, \delta[\mu - (t\sin\phi + 1)\tilde{k}] \\ &= \frac{8}{\pi}\int_{\mu/(t+1)}^{\Lambda} \tilde{k}\, d\tilde{k} \int_{[(\mu/\Lambda)-1](1/t)}^{1} \sqrt{1-x^2}dx\, \delta[\mu - (tx+1)\tilde{k}] \\ &= \frac{8\mu}{\pi}\int_{[(\mu/\Lambda)-1](1/t)}^{1} \frac{\sqrt{1-x^2}}{(tx+1)^2}dx\, \Theta\Big[\Lambda - \frac{\mu}{t+1}\Big].\end{aligned} \tag{B34}$$

Similarly, for $\lambda = -1$, $\Gamma_{xx}^{\mathrm{D},-}(\mu, t, \Lambda)$ reads

$$\Gamma_{xx}^{\mathrm{D},-}(\mu, t, \Lambda) = \frac{8\mu}{\pi}\int_{[(\mu/\Lambda)+1](1/t)}^{1} \frac{\sqrt{1-x^2}}{(tx-1)^2}dx\, \Theta\Big[\Lambda - \frac{\mu}{t-1}\Big]. \tag{B35}$$

As a consequence, $\Gamma_{xx}^{\mathrm{D}}(\mu, t, \Lambda)$ can be written as

$$\begin{aligned}\Gamma_{xx}^{\mathrm{D}}(\mu, t, \Lambda) &= \Gamma_{xx}^{\mathrm{D},-}(\mu, t, \Lambda) + \Gamma_{xx}^{\mathrm{D},+}(\mu, t, \Lambda) \\ &= \frac{8\mu}{\pi}\left\{\int_{[(\mu/\Lambda)-1](1/t)}^{1} \frac{\sqrt{1-x^2}}{(tx+1)^2}dx\, \Theta\Big[\Lambda - \frac{\mu}{t+1}\Big] + \int_{[(\mu/\Lambda)+1](1/t)}^{1} \frac{\sqrt{1-x^2}}{(tx-1)^2}dx\, \Theta\Big[\Lambda - \frac{\mu}{t-1}\Big]\right\} \\ &= \frac{8\mu}{\pi}\left[A(\mu, t, \Lambda)\frac{2\Lambda}{\mu} + \frac{B(\mu, t, \Lambda)}{\sqrt{t^2-1}} - C(\mu, t, \Lambda)\right],\end{aligned} \tag{B36}$$

where

$$A(\mu,t,\Lambda)=\sum_{\chi=\pm}\frac{1}{2t}\sqrt{1-\left(\frac{\mu-\chi\Lambda}{t\Lambda}\right)^2},$$

$$B(\mu,t,\Lambda)=\frac{1}{t^2}\ln\frac{t^2+\frac{\mu-\Lambda}{\Lambda}+\sqrt{t^2-1}\sqrt{t^2-(\frac{\mu-\Lambda}{\Lambda})^2}}{t^2-\frac{\mu+\Lambda}{\Lambda}+\sqrt{t^2-1}\sqrt{t^2-(\frac{\mu+\Lambda}{\Lambda})^2}},$$

$$C(\mu,t,\Lambda)=\sum_{\chi=\pm}\frac{1}{t^2}\arccos\frac{\mu-\chi\Lambda}{t\Lambda}. \tag{B37}$$

Similarly, $\Gamma^{\mathrm{D}}_{yy}(\mu,t,\Lambda)$ can be written as

$$\begin{aligned}\Gamma^{\mathrm{D}}_{yy}(\mu,t,\Lambda)&=\Gamma^{\mathrm{D},+}_{yy}(\mu,t,\Lambda)+\Gamma^{\mathrm{D},-}_{yy}(\mu,t,\Lambda)\\&=\frac{8\mu}{\pi}\left\{\int^1_{[(\mu/\Lambda)-1](1/t)}\frac{1}{(1+tx)^2}\frac{(x+t)^2}{\sqrt{1-x^2}}dx\,\Theta\Big[\Lambda-\frac{\mu}{1+t}\Big]+\int^1_{[(\mu/\Lambda)+1](1/t)}\frac{1}{(tx-1)^2}\frac{(x-t)^2}{\sqrt{1-x^2}}dx\,\Theta\Big[\Lambda-\frac{\mu}{t-1}\Big]\right\}\\&=\frac{8\mu}{\pi}\left[(t^2-1)A(\mu,t,\Lambda)\frac{2\Lambda}{\mu}+\sqrt{t^2-1}B(\mu,t,\Lambda)+C(\mu,t,\Lambda)\right].\end{aligned} \tag{B38}$$

Keeping the order of $O(1)$ of Λ, we have

$$\Gamma^{\mathrm{D}}_{xx}(\mu,t,\Lambda)=8\mu\left[\frac{\sqrt{t^2-1}}{\pi t^2}\frac{2\Lambda}{\mu}-\frac{1}{t^2}\right], \tag{B39}$$

$$\Gamma^{\mathrm{D}}_{yy}(\mu,t,\Lambda)=8\mu\left[\frac{\sqrt{(t^2-1)^3}}{\pi t^2}\frac{2\Lambda}{\mu}+\frac{1}{t^2}\right]. \tag{B40}$$

c. Intraband LOC for type-III phase

For the type-III phase ($t=1$), $\Gamma^{\mathrm{D},\mathrm{sgn}(\mu)}_{xx}(\mu,t,\Lambda)$ and $\Gamma^{\mathrm{D},\mathrm{sgn}(\mu)}_{yy}(\mu,t,\Lambda)$ can be given by

$$\begin{aligned}\Gamma^{\mathrm{D},\mathrm{sgn}(\mu)}_{xx}(\mu,t,\Lambda)&=\frac{8\mu}{\pi}\int^1_{(\mu/\Lambda)-1}\frac{\sqrt{1-x^2}}{(1+x)^2}dx\,\Theta\Big[\Lambda-\frac{\mu}{2}\Big]=\frac{16\mu}{\pi}\left[\sqrt{\frac{2\Lambda}{\mu}-1}-\arccos\sqrt{\frac{\mu}{2\Lambda}}\right]\\&=\frac{16\mu}{\pi}\left[\sqrt{\frac{2\Lambda-\mu}{\mu}}-\arccos\sqrt{\frac{\mu}{2\Lambda}}\right],\end{aligned} \tag{B41}$$

$$\begin{aligned}\Gamma^{\mathrm{D},\mathrm{sgn}(\mu)}_{yy}(\mu,t,\Lambda)&=\frac{8\mu}{\pi}\int^1_{(\mu/\Lambda)-1}\frac{1}{(1+x)^2}\frac{(x+1)^2}{\sqrt{1-x^2}}dx\,\Theta\Big[\Lambda-\frac{\mu}{2}\Big]=\frac{8\mu}{\pi}\arccos\left(\frac{\mu}{\Lambda}-1\right)\\&=\frac{8\mu}{\pi}\arccos\left(\frac{\mu-\Lambda}{\Lambda}\right).\end{aligned} \tag{B42}$$

Keeping the order of $O(1)$ of Λ, we have

$$\Gamma^{\mathrm{D},\mathrm{sgn}(\mu)}_{xx}(\mu,t,\Lambda)=\frac{16\mu}{\pi}\left[\sqrt{\frac{2\Lambda-\mu}{\mu}}-\arccos\sqrt{\frac{\mu}{2\Lambda}}\right]=8\mu\left[\frac{2}{\pi}\sqrt{\frac{2\Lambda}{\mu}}-1\right] \tag{B43}$$

and

$$\Gamma^{\mathrm{D},\mathrm{sgn}(\mu)}_{yy}(\mu,t,\Lambda)=\frac{8\mu}{\pi}\arccos\left(\frac{\mu-\Lambda}{\Lambda}\right)=8\mu. \tag{B44}$$

APPENDIX C: DETAILED CALCULATION OF JDOS

In the following, we present the detailed calculation of JDOS in the n-doped case [$\mu>0$, namely, $\mathrm{sgn}(\mu)=+$] for the type-I, type-II, and type-III Dirac bands.

1. Calculation of JDOS for type-I phase

For the type-I phase ($0<t<1$), the conduction band is partially occupied by electrons, and the Fermi wave vectors are $\tilde{k}^{\kappa,+}_F(\mu)=\mu/(\kappa t\sin\phi+1)$. Due to the Pauli blocking, the energy of the photon must excite electrons from the valence band to

the conduction band above the Fermi surface, which requires $\omega \geqslant \tilde{\varepsilon}_{\kappa}^{+}[\tilde{k}_F^{\kappa,+}(\mu)] - \tilde{\varepsilon}_{\kappa}^{-}[\tilde{k}_F^{\kappa,+}(\mu)] = 2\tilde{k}_F^{\kappa,+}(\mu) = 2\mu/(\kappa t \sin\phi + 1)$ with $\phi \in [0, 2\pi]$. The JDOS at the $+\kappa$ valley can be written as

$$\begin{aligned}
\mathcal{J}_{\kappa}(\omega) &= \frac{\mathcal{J}_0}{2\pi}\int_0^{+\infty}\tilde{k}\,d\tilde{k}\int_0^{2\pi}d\phi\,\delta(2\tilde{k}-\omega)\Theta\big[\omega - 2\tilde{k}_F^{\kappa,+}(\mu)\big] \\
&= \frac{\mathcal{J}_0}{2\pi}\int_0^{+\infty}\tilde{k}\,d\tilde{k}\int_0^{2\pi}d\phi\,\delta(2\tilde{k}-\omega)\Theta\left[\omega - \frac{2\mu}{\kappa t\sin\phi+1}\right] \\
&= \mathcal{J}_0\frac{\omega}{8\pi}\int_{-\pi/2}^{3\pi/2}d\phi\,\Theta\left[\omega - \frac{2\mu}{\kappa t\sin\phi+1}\right] \\
&= \mathcal{J}_0\frac{\omega}{8\pi}\int_{-\pi/2}^{\pi/2}d\phi\left\{\Theta\left[\omega - \frac{2\mu}{\kappa t\sin\phi+1}\right] + \Theta\left[\omega - \frac{2\mu}{-\kappa t\sin\phi+1}\right]\right\} = \mathcal{J}_{-\kappa}(\omega).
\end{aligned} \tag{C1}$$

As a result, $\mathcal{J}(\omega) = g_s g_v \mathcal{J}_{\kappa}(\omega)$, where $g_v = 2$ denotes the valley degeneracy. After introducing $x = \sin\phi$, one can obtain

$$\begin{aligned}
\mathcal{J}(\omega) = g_s g_v \mathcal{J}_{\kappa}(\omega) &= \mathcal{J}_0\frac{\omega}{2\pi}\int_{-1}^{1}\frac{dx}{\sqrt{1-x^2}}\left\{\Theta\left[\omega - \frac{2\mu}{tx+1}\right] + \Theta\left[\omega - \frac{2\mu}{-tx+1}\right]\right\} \\
&= \mathcal{J}_0\frac{\omega}{\pi}\int_{-1}^{1}\frac{dx}{\sqrt{1-x^2}}\Theta\left[\omega - \frac{2\mu}{tx+1}\right] = \mathcal{J}_0\omega\begin{cases}0, & 0<\omega<\omega_1(t)\\ \frac{\arccos\xi_-}{\pi}, & \omega_1(t)\leqslant\omega<\omega_2(t)\\ 1, & \omega\geqslant\omega_2(t),\end{cases}
\end{aligned} \tag{C2}$$

where

$$\xi_{\pm} = \frac{2\mu \pm \omega}{\omega}\frac{\Theta(t)}{t}, \tag{C3}$$

$$\omega_1(t) = 2\mu\frac{\Theta(t)}{1+t}, \tag{C4}$$

$$\omega_2(t) = 2\mu\left[\frac{\Theta(1-t)}{1-t} + \frac{\Theta(t-1)}{t-1}\right]. \tag{C5}$$

In addition, it is easy to obtain for the untilted case ($t = 0$) that

$$\mathcal{J}(\omega) = \mathcal{J}_0\frac{\omega}{2\pi}\int_0^{2\pi}d\phi\,\Theta[\omega - 2\mu] = \mathcal{J}_0\omega\begin{cases}0, & 0<\omega<2\mu\\ 1, & \omega\geqslant 2\mu.\end{cases} \tag{C6}$$

2. Calculation of JDOS for type-II phase

For the type-II phase ($t > 1$), the valence band is partially occupied by holes, and the electron transition area will be restricted by a valence band and a conduction band. In order to conveniently describe the integration area of JDOS in $\tilde{k}$ space, we introduce two angle parameters ϕ_1 and ϕ_2, which are obtained by solving $(t\sin\phi_1 + 1)\Lambda = \mu$ and $(t\sin\phi_2 - 1)\Lambda = \mu$, respectively, where Λ is the cutoff of $\tilde{k}$, as shown in Fig. 5. The photon energy contributed to the LOC is limited to $2\tilde{k}_F^{\kappa,+}(\mu) \leqslant \omega \leqslant 2\tilde{k}_F^{\kappa,-}(\mu)$.

In the polar coordinate, the JDOS for the $\kappa = +$ valley and the $\kappa = -$ valley can be respectively written as

$$\begin{aligned}
\mathcal{J}_{+}(\omega) &= \frac{\mathcal{J}_0}{2\pi}\left\{\int_{\mu/(t+1)}^{\Lambda}\tilde{k}\,d\tilde{k}\int_{\phi_1}^{\pi+|\phi_1|}d\phi\,\delta(2\tilde{k}-\omega)\Theta[\omega - 2\tilde{k}_F^{+,+}(\mu)] - \int_{\mu/(t-1)}^{\Lambda}\tilde{k}\,d\tilde{k}\int_{\phi_2}^{\pi-\phi_2}d\phi\,\delta(2\tilde{k}-\omega)\Theta[\omega - 2\tilde{k}_F^{+,-}(\mu)]\right\} \\
&= \frac{\mathcal{J}_0}{2\pi}\left\{\int_{\mu/(t+1)}^{\Lambda}\tilde{k}\,d\tilde{k}\int_{\phi_1}^{\pi+|\phi_1|}d\phi\,\delta(2\tilde{k}-\omega)\Theta\left[\omega - \frac{2\mu}{t\sin\phi+1}\right] - \int_{\mu/(t-1)}^{\Lambda}\tilde{k}\,d\tilde{k}\int_{\phi_2}^{\pi-\phi_2}d\phi\,\delta(2\tilde{k}-\omega)\Theta\left[\omega - \frac{2\mu}{t\sin\phi-1}\right]\right\} \\
&= \frac{\mathcal{J}_0}{\pi}\left\{\int_{\mu/(t+1)}^{\Lambda}\tilde{k}\,d\tilde{k}\int_{\phi_1}^{\pi/2}d\phi\,\delta(2\tilde{k}-\omega)\Theta\left[\omega - \frac{2\mu}{t\sin\phi+1}\right] - \int_{\mu/(t-1)}^{\Lambda}\tilde{k}\,d\tilde{k}\int_{\phi_2}^{\pi/2}d\phi\,\delta(2\tilde{k}-\omega)\Theta\left[\omega - \frac{2\mu}{t\sin\phi-1}\right]\right\}
\end{aligned} \tag{C7}$$

and

$$\begin{aligned}
\mathcal{J}_{-}(\omega) = \frac{\mathcal{J}_0}{\pi}\Bigg\{&\int_{\mu/(t+1)}^{\Lambda}\tilde{k}\,d\tilde{k}\int_{-\pi/2}^{-\phi_1}d\phi\,\delta(2\tilde{k}-\omega)\Theta\left[\omega - \frac{2\mu}{-t\sin\phi+1}\right] \\
&- \int_{\mu/(t-1)}^{\Lambda}\tilde{k}\,d\tilde{k}\int_{-\pi/2}^{-\phi_2}d\phi\,\delta(2\tilde{k}-\omega)\Theta\left[\omega - \frac{2\mu}{-t\sin\phi-1}\right]\Bigg\},
\end{aligned} \tag{C8}$$

where $\Theta[\Lambda - \frac{\mu}{t+1}]$ and $\Theta[\Lambda - \frac{\mu}{t-1}]$ are omitted here.

By replacing $\sin\phi$ with x and integrating over $\tilde{k}$, we get

$$\begin{aligned}\mathcal{J}(\omega) =& g_s[\mathcal{J}_+(\omega)+\mathcal{J}_-(\omega)]\\ =& g_s\Bigg[\mathcal{J}_0\frac{\omega}{4\pi}\left\{\int_{[(\mu/\Lambda)-1](1/t)}^{1}\frac{dx}{\sqrt{1-x^2}}\Theta\left[\omega-\frac{2\mu}{|tx+1|}\right]-\int_{[(\mu/\Lambda)+1](1/t)}^{1}\frac{dx}{\sqrt{1-x^2}}\Theta\left[\omega-\frac{2\mu}{|tx-1|}\right]\right\}\\ &+\mathcal{J}_0\frac{\omega}{4\pi}\left\{\int_{-1}^{-[(\mu/\Lambda)-1](1/t)}\frac{dx}{\sqrt{1-x^2}}\Theta\left[\omega-\frac{2\mu}{-tx+1|}\right]-\int_{-1}^{-[(\mu/\Lambda)+1](1/t)}\frac{dx}{\sqrt{1-x^2}}\Theta\left[\omega-\frac{2\mu}{-tx-1}\right]\right\}\Bigg]\\ =& \mathcal{J}_0\frac{\omega}{\pi}\left\{\int_{[(\mu/\Lambda)-1](1/t)}^{1}\frac{dx}{\sqrt{1-x^2}}\Theta\left[\omega-\frac{2\mu}{tx+1}\right]-\int_{[(\mu/\Lambda)+1](1/t)}^{1}\frac{dx}{\sqrt{1-x^2}}\Theta\left[\omega-\frac{2\mu}{tx-1}\right]\right\}\\ =& \mathcal{J}_0\frac{\omega}{\pi}\begin{cases}0, & \omega<\omega_1(t)\\ \arccos\xi_-, & \omega_1(t)\leqslant\omega<\omega_2(t)\\ \arcsin\xi_+-\arcsin\xi_-, & \omega\geqslant\omega_2(t).\end{cases}\end{aligned}\tag{C9}$$

3. Calculation of JDOS for type-III phase

For the type-III phase ($t=1$), we can easily obtain that

$$\begin{aligned}\mathcal{J}(\omega) =& \mathcal{J}_0\frac{\omega}{2\pi}\int_{(\mu/\Lambda)-1}^{1}\frac{dx}{\sqrt{1-x^2}}\Theta\left[\omega-\frac{2\mu}{x+1}\right]+\mathcal{J}_0\frac{\omega}{2\pi}\int_{-1}^{-[(\mu/\Lambda)-1]}\frac{dx}{\sqrt{1-x^2}}\Theta\left[\omega-\frac{2\mu}{-x+1}\right]\\ =& \mathcal{J}_0\frac{\omega}{\pi}\int_{(\mu/\Lambda)-1}^{1}\frac{dx}{\sqrt{1-x^2}}\Theta\left[\omega-\frac{2\mu}{x+1}\right]=\mathcal{J}_0\frac{\omega}{\pi}\begin{cases}0, & \omega<\mu\\ \arccos\xi_-, & \omega\geqslant\mu.\end{cases}\end{aligned}\tag{C10}$$

APPENDIX D: THE RELATIONSHIP BETWEEN JDOS AND THE INTERBAND LOCs

In this Appendix we will give the connection between the interband part of the optical conductivity $\mathrm{Re}\sigma_{jj}^{\mathrm{IB}}(\omega)$ and the JDOS. For the convenience of the following elaboration, we introduce a temporary auxiliary function $\mathcal{J}_L(\omega)$. The JDOS can be written as $\mathcal{J}(\omega)=(\omega\mathcal{J}_0)\times\mathcal{J}_L(\omega)$.

The complete formalisms for $\mathrm{Re}\sigma_{xx}^{\kappa}(\omega)$ and $\mathrm{Re}\sigma_{yy}^{\kappa}(\omega)$ are as follows (at zero temperature $T\to 0$):

$$\begin{aligned}\mathrm{Re}\sigma_{xx}^{\kappa(\mathrm{IB})}(\omega) =& 2\sigma_0 v_x^2\pi\int\frac{d^2\boldsymbol{k}}{(2\pi)^2}\left\{1-\frac{v_x^2k_x^2-v_y^2k_y^2}{[\mathcal{Z}(k_x,k_y)]^2}\right\}\frac{\Theta[\mu-\varepsilon_\kappa^-(k_x,k_y)]-\Theta[\mu-\varepsilon_\kappa^+(k_x,k_y)]}{\omega}\delta[\omega-2\mathcal{Z}(k_x,k_y)]\\ =& 2\sigma_0 v_x^2\pi\left\{\frac{\mathcal{J}_\kappa(\omega)}{\omega}-\int\frac{d^2\boldsymbol{k}}{(2\pi)^2}\frac{v_x^2k_x^2-v_y^2k_y^2}{[\mathcal{Z}(k_x,k_y)]^2}\frac{\Theta[\mu-\varepsilon_\kappa^-(k_x,k_y)]-\Theta[\mu-\varepsilon_\kappa^+(k_x,k_y)]}{\omega}\delta[\omega-2\mathcal{Z}(k_x,k_y)]\right\}\\ =& \sigma_0\left[2v_x^2\pi\frac{\mathcal{J}_\kappa(\omega)}{\omega}-\frac{v_x}{v_y}\mathcal{L}_\kappa(\omega)\right],\end{aligned}\tag{D1}$$

$$\begin{aligned}\mathrm{Re}\sigma_{yy}^{\kappa(\mathrm{IB})}(\omega) =& 2\sigma_0 v_y^2\pi\int\frac{d^2\boldsymbol{k}}{(2\pi)^2}\left\{1+\frac{v_x^2k_x^2-v_y^2k_y^2}{[\mathcal{Z}(k_x,k_y)]^2}\right\}\frac{\Theta[\mu-\varepsilon_\kappa^-(k_x,k_y)]-\Theta[\mu-\varepsilon_\kappa^+(k_x,k_y)]}{\omega}\delta[\omega-2\mathcal{Z}(k_x,k_y)]\\ =& \sigma_0\left[2v_y^2\pi\frac{\mathcal{J}_\kappa(\omega)}{\omega}+\frac{v_y}{v_x}\mathcal{L}_\kappa(\omega)\right],\end{aligned}\tag{D2}$$

where

$$\mathcal{L}_\kappa(\omega)=2\pi v_xv_y\int\frac{d^2\boldsymbol{k}}{(2\pi)^2}\frac{v_x^2k_x^2-v_y^2k_y^2}{[\mathcal{Z}(k_x,k_y)]^2}\frac{\Theta[\mu-\varepsilon_\kappa^-(k_x,k_y)]-\Theta[\mu-\varepsilon_\kappa^+(k_x,k_y)]}{\omega}\delta[\omega-2\mathcal{Z}(k_x,k_y)].\tag{D3}$$

The final formalism for $\mathrm{Re}\sigma_{jj}^{\mathrm{IB}}(\omega)$ are

$$\begin{aligned}\mathrm{Re}\sigma_{xx}^{\mathrm{IB}}(\omega) =& g_s\sum_{\kappa=\pm1}\mathrm{Re}\sigma_{xx}^{\kappa(\mathrm{IB})}(\omega)=\sigma_0\left[2v_x^2\pi g_s\sum_{\kappa=\pm1}\frac{\mathcal{J}_\kappa(\omega)}{\omega}-g_s\sum_{\kappa=\pm1}\frac{v_x}{v_y}\mathcal{L}_\kappa(\omega)\right]\\ =& \sigma_0\left[2v_x^2\pi\frac{\mathcal{J}(\omega)}{\omega}-\frac{v_x}{v_y}\mathcal{L}(\omega)\right]=\sigma_0\left[\frac{2v_x^2\pi}{\omega}(\omega\mathcal{J}_0)\mathcal{J}_L(\omega)-\frac{v_x}{v_y}\mathcal{L}(\omega)\right]\\ =& \sigma_0\left[\frac{2v_x^2\pi}{\omega}\frac{\omega}{2\pi v_xv_y}\mathcal{J}_L(\omega)-\frac{v_x}{v_y}\mathcal{L}(\omega)\right]=\sigma_0\frac{v_x}{v_y}[\mathcal{J}_L(\omega)-\mathcal{L}(\omega)]=\sigma_0\frac{v_x}{v_y}\left[\frac{\mathcal{J}(\omega)}{\mathcal{J}_0\omega}+\mathcal{L}(\omega)\right],\end{aligned}\tag{D4}$$

$$\mathrm{Re}\sigma_{yy}^{\mathrm{IB}}(\omega) = g_s \sum_{\kappa=\pm1} \mathrm{Re}\sigma_{yy}^{\kappa(\mathrm{IB})}(\omega) = \sigma_0 \left[2v_x^2 \pi \frac{\mathcal{J}(\omega)}{\omega} + \frac{v_y}{v_x} \mathcal{L}(\omega) \right]$$
$$= \sigma_0 \frac{v_y}{v_x} [\mathcal{J}_L(\omega) + \mathcal{L}(\omega)] = \sigma_0 \frac{v_y}{v_x} \left[\frac{\mathcal{J}(\omega)}{\mathcal{J}_0 \omega} + \mathcal{L}(\omega) \right], \tag{D5}$$

namely,

$$\Gamma_{xx}^{\mathrm{IB}}(\omega) = \frac{\mathcal{J}(\omega)}{\mathcal{J}_0 \omega} - \mathcal{L}(\omega),$$
$$\Gamma_{yy}^{\mathrm{IB}}(\omega) = \frac{\mathcal{J}(\omega)}{\mathcal{J}_0 \omega} + \mathcal{L}(\omega), \tag{D6}$$

where

$$\mathcal{L}(\omega) = g_s \sum_{\kappa=\pm1} \mathcal{L}_\kappa(\omega). \tag{D7}$$

After analysis and calculation similar to $\mathrm{Re}\sigma_{jj}(\omega)$, we can get

$$\mathcal{L}(\omega) = \frac{1}{\pi} \int_{-1}^{1} \frac{1-2x^2}{\sqrt{1-x^2}} dx \{\Theta[-x+\xi_+] - \Theta[-x+\xi_-]\}. \tag{D8}$$

Using the approach discussed in Appendix B for the Heaviside step functions at different tilt types, we can obtain analytical results for $\mathcal{L}(\omega)$. For type-I phase ($0 < t < 1$), the analytical expression of $\mathcal{L}(\omega)$ is given as

$$\mathcal{L}(\omega) = \frac{1}{\pi} \begin{cases} 0, & 0 < \omega < \omega_1(t) \\ -\xi_- \sqrt{1-\xi_-^2}, & \omega_1(t) \leqslant \omega < \omega_2(t) \\ 0, & \omega \geqslant \omega_2(t). \end{cases} \tag{D9}$$

For the type-II phase ($t > 1$), the analytical expression of $\mathcal{L}(\omega)$ takes the form

$$\mathcal{L}(\omega) = \frac{1}{\pi} \begin{cases} 0, & 0 < \omega < \omega_1(t) \\ -\xi_- \sqrt{1-\xi_-^2}, & \omega_1(t) \leqslant \omega < \omega_2(t) \\ \xi_+ \sqrt{1-\xi_+^2} - \xi_- \sqrt{1-\xi_-^2}, & \omega \geqslant \omega_2(t). \end{cases} \tag{D10}$$

For the type-III phase ($t = 1$), the auxiliary function $\mathcal{L}(\omega)$ can be written as

$$\mathcal{L}(\omega) = \frac{1}{\pi} \begin{cases} 0, & 0 < \omega < \mu \\ -\xi_- \sqrt{1-\xi_-^2}, & \omega \geqslant \mu. \end{cases} \tag{D11}$$

[1] K. S. Novoselov, A. K. Geim, S. V. Morozov, D. Jiang, Y. Zhang, S. V. Dubonos, I. V. Grigorieva, and A. A. Firsov, Science **306**, 666 (2004).

[2] A. H. Castro Neto, F. Guinea, N. M. R. Peres, K. S. Novoselov, and A. K. Geim, Rev. Mod. Phys. **81**, 109 (2009).

[3] S. Katayama, A. Kobayashi, and Y. Suzumura, J. Phys. Soc. Jpn. **75**, 054705 (2006).

[4] G. G. Guzman-Verri and L. C. Lew Yan Voon, Phys. Rev. B **76**, 075131 (2007).

[5] S. Cahangirov, M. Topsakal, E. Aktürk, H. Şahin, and S. Ciraci, Phys. Rev. Lett. **102**, 236804 (2009).

[6] C.-C. Liu, H. Jiang, and Y. Yao, Phys. Rev. B **84**, 195430 (2011).

[7] C.-C. Liu, W. Feng, and Y. Yao, Phys. Rev. Lett. **107**, 076802 (2011).

[8] M. Ezawa, Phys. Rev. Lett. **109**, 055502 (2012).

[9] S. M. Choi, S. H. Jhi, and Y. W. Son, Phys. Rev. B **81**, 081407(R) (2010).

[10] X. F. Zhou, X. Dong, A. R. Oganov, Q. Zhu, Y. J. Tian, and H. T. Wang, Phys. Rev. Lett. **112**, 085502 (2014).

[11] A. J. Mannix, X.-F. Zhou, B. Kiraly, J. D. Wood, D. Alducin, B. D. Myers, X. Liu, B. L. Fisher, U. Santiago, J. R. Guest, M. J. Yacaman, A. Ponce, A. R. Oganov, M. C. Hersam, and N. P. Guisinger, Science **350**, 1513 (2015).

[12] A. Lopez-Bezanilla and P. B. Littlewood, Phys. Rev. B **93**, 241405(R) (2016).

[13] A. D. Zabolotskiy and Yu. E. Lozovik, Phys. Rev. B **94**, 165403 (2016).

[14] K. F. Mak, C. Lee, J. Hone, J. Shan, and T. F. Heinz, Phys. Rev. Lett. **105**, 136805 (2010).

[15] D. Xiao, G. B. Liu, W. Feng, X. Xu, and W. Yao, Phys. Rev. Lett. **108**, 196802 (2012).

[16] X. Qian, J. Liu, L. Fu, and J. Li, Science **346**, 1344 (2014).
[17] H. Y. Lu, A. S. Cuamba, S. Y. Lin, L. Hao, R. Wang, H. Li, Y. Y. Zhao, and C. S. Ting, Phys. Rev. B **94**, 195423 (2016).
[18] Y. Ma, L. Kou, X. Li, Y. Dai, and T. Heine, NPG Asia Mater. **8**, e264 (2016).
[19] S. Li, Y. Liu, Z.-M. Yu, Y. Jiao, S. Guan, X.-L. Sheng, Y. Yao, and S. A. Yang, Phys. Rev. B **100**, 205102 (2019).
[20] P.-J. Guo, X.-Q. Lu, W. Ji, K. Liu, and Z.-Y. Lu, Phys. Rev. B **102**, 041109(R) (2020).
[21] T. Nishine, A. Kobayashi, and Y. Suzumura, J. Phys. Soc. Jpn. **80**, 114713 (2011).
[22] T. Nishine, A. Kobayashi, and Y. Suzumura, J. Phys. Soc. Jpn. **79**, 114715 (2010).
[23] A. Iurov, G. Gumbs, D. Huang, and G. Balakrishnan, Phys. Rev. B **96**, 245403 (2017).
[24] K. Sadhukhan and A. Agarwal, Phys. Rev. B **96**, 035410 (2017).
[25] Z. Jalali-Mola and S. A. Jafari, Phys. Rev. B **98**, 195415 (2018).
[26] M. A. Mojarro, R. Carrillo-Bastos, and Jesús A. Maytorena, Phys. Rev. B **105**, L201408 (2022).
[27] S. Verma, A. Mawrie, and T. K. Ghosh, Phys. Rev. B **96**, 155418 (2017).
[28] S. A. Herrera and G. G. Naumis, Phys. Rev. B **100**, 195420 (2019).
[29] S. Rostamzadeh, İ. Adagideli, and M. O. Goerbig, Phys. Rev. B **100**, 075438 (2019).
[30] C.-Y. Tan, C.-X. Yan, Y.-H. Zhao, H. Guo, and H.-R. Chang, Phys. Rev. B **103**, 125425 (2021).
[31] M. A. Mojarro, R. Carrillo-Bastos, and Jesús A. Maytorena, Phys. Rev. B **103**, 165415 (2021).
[32] H. Yao, M. Zhu, L. Jiang, and Y. Zheng, Phys. Rev. B **104**, 235406 (2021).
[33] A. Iurov, G. Gumbs, and D. Huang, Phys. Rev. B **98**, 075414 (2018).
[34] A. Iurov, L. Zhemchuzhna, D. Dahal, G. Gumbs, and D. Huang, Phys. Rev. B **101**, 035129 (2020).
[35] SK. Firoz Islam and A. M. Jayannavar, Phys. Rev. B **96**, 235405 (2017).
[36] D. Li, B. Rosenstein, B. Ya. Shapiro, and I. Shapiro, Phys. Rev. B **95**, 094513 (2017).
[37] S. H. Zhang and W. Yang, Phys. Rev. B **97**, 235440 (2018).
[38] V. H. Nguyen and J. C. Charlier, Phys. Rev. B **97**, 235113 (2018).
[39] F. Qi and X. Zhou, Chin. Phys. B **31**, 077301 (2022).
[40] J.-H. Sun, L.-J. Wang, X.-T. Hu, L. Li, and D.-H. Xu, Phys. Rev. B **97**, 035130 (2018).
[41] G. C. Paul, SK Firoz Islam, and A. Saha, Phys. Rev. B **99**, 155418 (2019).
[42] S.-H. Zhang, D.-F. Shao, and W. Yang, J. Magn. Magn. Mater. **491**, 165631 (2019).
[43] S.-H. Zheng, H.-J. Duan, J.-K. Wang, J.-Y. Li, M.-X. Deng, and R.-Q. Wang, Phys. Rev. B **101**, 041408(R) (2020).
[44] H. Rostami and V. Juričić, Phys. Rev. Res. **2**, 013069 (2020).
[45] P. Kapri, B. Dey, and T. K. Ghosh, Phys. Rev. B **102**, 045417 (2020).
[46] P. Sengupta and E. Bellotti, Appl. Phys. Lett. **117**, 223103 (2020).
[47] J. Zheng, J. Lu, and F. Zhai, Nanotechnology **32**, 025205 (2021).
[48] T. Farajollahpour and S. A. Jafari, Phys. Rev. Res. **2**, 023410 (2020).
[49] Z. Faraei and S. A. Jafari, Phys. Rev. B **101**, 214508 (2020).
[50] W. Fu, S.-S. Ke, M.-X. Lu, and H.-F. Lv, Phys. E **134**, 114841 (2021).
[51] R. A. Ng, A. Wild, M. E. Portnoi, and R. R. Hartmann, Sci. Rep. **12**, 7688 (2022).
[52] Yonatan Betancur-Ocampo, E. Díaz-Bautista, and Thomas Stegmann, Phys. Rev. B **105**, 045401 (2022).
[53] I. M. Lifshitz, Sov. Phys. J. Exptl. Theoret. Phys. **11**, 1130 (1960).
[54] Z. J. Xiang, G. J. Ye, C. Shang, B. Lei, N. Z. Wang, K. S. Yang, D. Y. Liu, F. B. Meng, X. G. Luo, L. J. Zou *et al.*, Phys. Rev. Lett. **115**, 186403 (2015).
[55] C. Liu, T. Kondo, R. M. Fernandes, A. D. Palczewski, E. D. Mun, N. Ni, A. N. Thaler, A. Bostwick, E. Rotenberg, J. Schmalian *et al.*, Nat. Phys. **6**, 419 (2010).
[56] Q.-Y. Wang, Z. Li, W.-H. Zhang, Z.-C. Zhang, J.-S. Zhang, W. Li, H. Ding, Y.-B. Ou, P. Deng, K. Chang *et al.*, Chin. Phys. Lett. **29**, 037402 (2012).
[57] Y. Wang, M. N. Gastiasoro, B. M. Andersen, M. Tomic, H. O. Jeschke, R. Valenti, I. Paul, and P. J. Hirschfeld, Phys. Rev. Lett. **114**, 097003 (2015).
[58] X. Shi, Z.-Q. Han, X.-L. Peng, P. Richard, T. Qian, X.-X. Wu, M.-W. Qiu, S. C. Wang, J. P. Hu, Y.-J. Sun *et al.*, Nat. Commun. **8**, 14988 (2017).
[59] M. Q. Ren, Y. J. Yan, X. H. Niu, R. Tao, D. Hu, R. Peng, B. Xie, J. Zhao, T. Zhang, and D.-L. Feng, Sci. Adv. **3**, e1603238 (2017).
[60] D. Aoki, G. Seyfarth, A. Pourret, A. Gourgout, A. McCollam, J. A. N. Bruin, Y. Krupko, and I. Sheikin, Phys. Rev. Lett. **116**, 037202 (2016).
[61] G. Bastien, A. Gourgout, D. Aoki, A. Pourret, I. Sheikin, G. Seyfarth, J. Flouquet, and G. Knebel, Phys. Rev. Lett. **117**, 206401 (2016).
[62] Y. Zhang, C. Wang, L. Yu, G. Liu, A. Liang, J. Huang, S. Nie, X. Sun, Y. Zhang, B. Shen *et al.*, Nat. Commun. **8**, 15512 (2017).
[63] F. Liu, J. Li, K. Zhang, S. Peng, H. Huang, M. Yan, N. Li, Q. Zhang, S. Guo, X. Lü *et al.*, Sci. China Phys. Mech. Astron. **62**, 48211 (2019).
[64] G. E. Volovik and K. Zhang, J. Low Temp. Phys. **189**, 276 (2017).
[65] G. E. Volovik, Phys. Usp. **61**, 89 (2018).
[66] F. Xiong, X. Han, and C. Honerkamp, Phys. Rev. B **104**, 115151 (2021).
[67] S. Tchoumakov, M. Civelli, and M. O. Goerbig, Phys. Rev. Lett. **117**, 086402 (2016).
[68] S. Tchoumakov, M. Civelli, and M. O. Goerbig, Phys. Rev. B **95**, 125306 (2017).
[69] A. A. Zyuzin and R. P. Tiwari, JETP Lett. **103**, 717 (2016).
[70] Y. Ferreiros, A. A. Zyuzin, and J. H. Bardarson, Phys. Rev. B **96**, 115202 (2017).
[71] S. Saha and S. Tewari, Eur. Phys. J. B **91**, 4 (2018).
[72] Z.-M. Yu, Y. Yao, and S. A. Yang, Phys. Rev. Lett. **117**, 077202 (2016).
[73] Z. Hou and Q.-F. Sun, Phys. Rev. B **96**, 155305 (2017).
[74] T. E. O'Brien, M. Diez, and C. W. J. Beenakker, Phys. Rev. Lett. **116**, 236401 (2016).
[75] K. Sonowal, A. Singh, and A. Agarwal, Phys. Rev. B **100**, 085436 (2019).

[76] K. Das and A. Agarwal, Phys. Rev. B **99**, 085405 (2019).
[77] K. Sadhukhan, A. Politano, and A. Agarwal, Phys. Rev. Lett. **124**, 046803 (2020).
[78] H. J. Duan, S. H. Zheng, R. Q. Wang, M. X. Deng, and M. Yang, Phys. Rev. B **99**, 165111 (2019).
[79] J. P. Carbotte, Phys. Rev. B **94**, 165111 (2016).
[80] S. P. Mukherjee and J. P. Carbotte, Phys. Rev. B **96**, 085114 (2017).
[81] Y. Tamashevich, Leone Di Mauro Villari, and M. Ornigotti, Phys. Rev. B **105**, 195102 (2022).
[82] T. Farajollahpour, Z. Faraei, and S. A. Jafari, Phys. Rev. B **99**, 235150 (2019).
[83] V. P. Gusynin, S. G. Sharapov, and J. P. Carbotte, Phys. Rev. B **75**, 165407 (2007).
[84] V. P. Gusynin, S. G. Sharapov, and J. P. Carbotte, Phys. Rev. Lett. **96**, 256802 (2006).
[85] S. A. Mikhailov and K. Ziegler, Phys. Rev. Lett. **99**, 016803 (2007).
[86] A. B. Kuzmenko, E. van Heumen, F. Carbone, and D. van der Marel, Phys. Rev. Lett. **100**, 117401 (2008).
[87] K. F. Mak, M. Y. Sfeir, Y. Wu, C. H. Lui, J. A. Misewich, and T. F. Heinz, Phys. Rev. Lett. **101**, 196405 (2008).
[88] T. Stauber, N. M. R. Peres, and A. K. Geim, Phys. Rev. B **78**, 085432 (2008).
[89] Z. Q. Li, E. A. Henriksen, Z. Jiang, Z. Hao, M. C. Martin, P. Kim, H. L. Stormer, and D. N. Basov, Nat. Phys. **4**, 532 (2008).
[90] L. Stille, C. J. Tabert, and E. J. Nicol, Phys. Rev. B **86**, 195405 (2012).
[91] Z. Li and J. P. Carbotte, Phys. Rev. B **86**, 205425 (2012).
[92] A. Carvalho, R. M. Ribeiro, and A. H. Castro Neto, Phys. Rev. B **88**, 115205 (2013).
[93] H. Rostami and R. Asgari, Phys. Rev. B **89**, 115413 (2014).
[94] P. DiPietro, F. M. Vitucci, D. Nicoletti, L. Baldassarre, P. Calvani, R. Cava, Y. S. Hor, U. Schade, and S. Lupi, Phys. Rev. B **86**, 045439 (2012).
[95] Z. Li and J. P. Carbotte, Phys. Rev. B **87**, 155416 (2013).
[96] X. Xiao and W. Wen, Phys. Rev. B **88**, 045442 (2013).
[97] Phillip E. C. Ashby and J. P. Carbotte, Phys. Rev. B **89**, 245121 (2014).
[98] A. Wild, E. Mariani, and M. E. Portnoi, Phys. Rev. B **105**, 205306 (2022).